



Open Archive Toulouse Archive Ouverte (OATAO)

OATAO is an open access repository that collects the work of Toulouse researchers and makes it freely available over the web where possible.

This is an author-deposited version published in: <http://oatao.univ-toulouse.fr/>
Eprints ID: 5509

To link to this article: DOI:10.1007/s00158-012-0784-6

URL: <http://dx.doi.org/10.1007/s00158-012-0784-6>

To cite this version: Bettebghor, Dimitri and Bartoli, Nathalie
Approximation of the critical buckling factor for composite panels. (2012)
Structural and Multidisciplinary Optimization. pp. 01-24. ISSN 1615-147X

Any correspondence concerning this service should be sent to the repository administrator: staff-oatao@inp-toulouse.fr

Approximation of the critical buckling factor for composite panels

D. Bettebghor · N. Bartoli

Abstract This article is concerned with the approximation of the critical buckling factor for thin composite plates. A new method to improve the approximation of this critical factor is applied based on its dependence with respect to lamination parameters and loading conditions. This method allows accurate approximation of the critical buckling factor for non-orthotropic laminates under complex combined loadings (including shear loading). The influence of the stacking sequence and loading conditions is extensively studied as well as properties of the critical buckling factor behavior (e.g concavity over tensor D or out-of-plane lamination parameters). Moreover, the critical buckling factor is numerically shown to be piecewise linear for orthotropic laminates under combined loading whenever shear remains low and it is also shown to be piecewise continuous in the general case. Based on the numerically observed behavior, a new scheme for the approximation is applied that separates each buckling mode and builds linear, polynomial or rational regressions for each mode. Results of this approach and applications to structural optimization are presented.

D. Bettebghor
Onera - The French Aerospace Lab
Aeroelasticity and Structural Dynamics Department
F-92260, Chatillon, France
E-mail: dimitri.bettebghor@onera.fr
ISAE-Sup'Aéro
Department of Mathematics, Computer Sciences and Control Engineering
BP 54032 31055, Toulouse, France
E-mail: dimitri.bettebghor@isae.fr

N. Bartoli
Onera - The French Aerospace Lab
F-31055, Toulouse, France
E-mail: nathalie.bartoli@onera.fr

Keywords Buckling · Lamination parameters · Piecewise polynomial regression

1 Introduction

Structural optimization for composite thin-walled structures often exhibits large computational times due to repetitive stability analysis. For composite structure made of thin plates or thin shallow shells (such as aircraft fuselage), buckling computation is of primary importance since it is one of the critical sizing constraints when minimizing the weight. This computational burden becomes even critical when we address laminated composites and when the stacking sequence is optimized. The prescribed orientations and the feasibility rules for stacking sequences make this kind of problems NP-complete. To solve such problems, one often goes to population-based heuristics (evolutionary algorithms, particle swarm optimization...) to address the discreteness of the design variables. Such methods require many evaluations to ensure that a reasonably good optimum has been found. Even though more and more computational resources are available today, these resources do not increase in such a way that the optimization of large-composite structures that include realistic constraints such as blending (ply's orientation continuity, [37]) can be easily performed. If we think of the maximization of the critical buckling factor for one sole reasonably thick laminated plate (2×30 plies for instance), the complexity of the problem is still not treated in a satisfactory way since in general heuristics never guarantee that we find the global optimum. If we think of an assembly of many plates reinforced by laminated composites stringers, complexity of the problem grows even more than exponentially. A realistic fuselage optimiza-

tion that include say 10,000 super-stiffeners, 100 load cases with a few super-stiffener design variables (geometric dimensions, stacking sequence) and a few different stability and strength criteria, such an optimization will require more than one million of buckling evaluations per optimization iteration (without any sensitivity analysis) it will also require finite elements analyses to redistribute internal loads for the overall structure (it also quite complicates the sensitivity analysis). If we think of a standard buckling analysis that lasts a few seconds, say one second, one sole iteration would take more than one week. In case such an optimization is based on gradient methods and requires a few dozens of iterations to converge, this amount of computations could still be handled. However, we can not sill guarantee that this optimum is global. To get to the optimal design, we would need a real mixed-integer non linear programming technique (branch-and-bound, Gomory's cuts) to include combinatorial constraints such that blending resulting in tremendous amounts of evaluations, several billions of buckling evaluation even for small structures. The motivation of approximation models to replace standard buckling analysis (performed through Rayleigh-Ritz methods or detailed finite element methods) is not thought as a replacement for an analysis considered as alone but with respect to that huge number of repetitive analyses.

To build such approximation models, one classical strategy uses a continuous representation of the in-plane and out-of-plane behaviors of the stacking sequence by means of either lamination parameters, polar invariant representation or directly A and D tensors terms. Lamination parameters are dimensionless quantities that only depend on the stacking sequence. Unlike A and D tensors, their use allows to treat exclusively the dependence with respect to stacking sequences and not to the material dependence. We distinguish in-plane lamination parameters (ξ_A), bending-stretching lamination parameters (ξ_B) and out-of-plane (or bending or flexural) lamination parameters (ξ_D), leading to 12 variables for arbitrary stacking sequences. This continuous relaxation offers a way to treat the optimization (for instance the maximization of the critical buckling factor of a laminate plate under a given loading) as a continuous one, reducing the number of evaluations needed to converge whenever the optimization problem is well posed (e.g convex). A good property of lamination parameters is that most classical objective functions have interesting optimization properties when evaluated over the lamination space, which happens to be convex. However, this continuous relaxation has two major drawbacks. First when a continuous optimum is found, it

usually does not match a discrete solution, there is no practical stacking sequence that gives these optimal lamination parameters. A new discrete optimization step is to be performed to identify a correct discrete solution and there is no evidence that the discrete optimum found by this step is the real discrete optimum. The other important drawback is that not all sizing constraints can be computed on the basis of lamination parameters. Some optimization constraints do need the real stacking sequence to be computed: mechanical constraints (first-ply failure...), feasibility constraints (contiguity of same orientations to avoid matrix cracking for instance). However, lamination parameters do provide a practical continuous representation of in-plane and out-of-plane behavior making possible to build approximation models of the expensive optimization constraints, such as buckling computations. Even though continuous optimization over lamination parameters is not performed, such an approximation model allows to perform discrete optimizations in a much more efficient way.

Since their first application to the design of composite in the seminal work of Miki ([32], [33]), where the author derives a graphical procedure to optimize stiffness properties, lamination parameters have been extensively studied and covered as a practical and convenient tool to optimize laminated composites. Early work by Miki allowed to bound the lamination space. Much work was also done in describing the dependence of the critical buckling factor in the lamination space: Grenested ([16], [18], [17]) or Walker [44] investigated the influence of lamination parameters for the critical buckling factor in different cases (pure shear loading, non-orthotropic laminates,...) through different approximation methods: orthotropic closed-form expressions, finite strip method, Rayleigh-Ritz method... Grenested found out that non-orthotropy decreases the critical buckling factor for uni-axial compression loading and in many situations the optimum in the lamination space belongs to the boundary previously described by Miki, corresponding to angle-ply laminate $[+\theta/-\theta]$ with continuous angle θ . However practical stacking sequences that satisfy manufacturability constraints are not orthotropic nor angle-ply stacking sequences. A lot of work was also done in applying directly the optimization problem in the lamination space and then get from the continuous optimum a discrete solution usually by means of genetic algorithms ([15], [20]). Lamination parameters associated to real practical stacking sequences of orientations $[0^\circ/45^\circ/-45^\circ/90^\circ]$ exhibit a fractal structure that was exploited in [40] to derive a fractal branch-and-bound method. The precise description

of the feasible set of lamination parameters and more specifically the coupling between in-plane lamination parameters and out-of-plane lamination parameters was solved in [13], [9], resulting into so-called compatibility equations that constrain the feasible space for out-of-plane lamination parameters based on the values of in-plane lamination parameters. These compatibility equations describe a convex feasible set and can be directly integrated into an optimization [23]. Regarding the area of building approximations of the critical buckling factor over lamination parameters, much work was done with the help of response surfaces (polynomial regression of degree 2) [42], [1], [20], Taylor-based first-order linear approximation [23], radial basis function under tension [24], [26], adaptive response surface [41]. The non-differentiability of the critical buckling factor with respect to lamination parameters, which was already noticed in a more general framework (see [35] or [12] for general results on critical buckling factor differentiability not specifically devoted to composite) does not seem to have been considered when building approximation models. Regarding potential property of the critical buckling factor well suited for optimization, concavity was cited in several references [6], but to the authors' knowledge, it has never been proved on a sound mathematical basis for the general case (arbitrary geometry, non-orthotropic laminate).

This paper aims at studying numerically some properties of the critical buckling factor that will ease the construction of accurate approximations to be used within an optimization process. The approximation of the critical buckling factor over lamination parameters is not restricted to continuous optimization over lamination parameters, since such an approximation can be used when the stacking is directly addressed as an optimization variable (genetic algorithms, simulated annealing, particle swarm optimization). In particular, we show that the critical buckling factor is concave over lamination parameters. We also give numerical evidence of the piecewise behavior of the critical buckling factor depending on the region of the input space. Based on this knowledge we apply a recent strategy to build piecewise approximation models developed in [7]. The behavior of the critical buckling factor both over lamination parameters and varying loading conditions is covered and the suggested scheme seems to be well suited to approximate such derivative-discontinuous functions, applications to optimization (maximization of the critical buckling factor) are also given.

2 Lamination parameters and feasible stacking sequences

We briefly recall here the definition of out-of-plane lamination parameters and the feasibility constraints for laminated composites that we use in this paper.

2.1 Out-of-plane lamination parameters

Consider a composite of given material characteristics E_1, E_2, G_{12} and ν_{12} . Note Q_{11}, Q_{22}, Q_{12} and Q_{66} the reduced stiffness's. The Tsai-Pagano parameters $(U_i)_{i=1\dots 5}$ (or material invariants) are defined as

$$\begin{pmatrix} U_1 \\ U_2 \\ U_3 \\ U_4 \\ U_5 \end{pmatrix} = \begin{pmatrix} 3/8 & 3/8 & 1/4 & 1/2 \\ 1/2 & -1/2 & 0 & 0 \\ 1/8 & 1/8 & -1/4 & -1/2 \\ 1/8 & 1/8 & 3/4 & -1/2 \\ 1/8 & 1/8 & -1/4 & 1/2 \end{pmatrix} \begin{pmatrix} Q_{11} \\ Q_{22} \\ Q_{12} \\ Q_{66} \end{pmatrix} \quad (1)$$

the out-of-plane (or bending) lamination parameters are defined as

$$\xi_D^{\{1,2,3\}} = \frac{12}{h^3} \int_{-h/2}^{h/2} \{\cos(2\theta(z)), \cos(4\theta(z)), \sin(2\theta(z))\} dz \quad (2)$$

Note that we do not consider ξ_D^4 since it vanishes when computed over stacking sequences made of $[0^\circ/45^\circ/90^\circ]$ orientations. Now recall that the D tensor is expressed as an affine function of the lamination parameters as follows.

$$D_{11} = \frac{h^3}{12} (U_1 + U_2 \xi_1^D + U_3 \xi_2^D) \quad (3)$$

$$D_{22} = \frac{h^3}{12} (U_1 - U_2 \xi_1^D + U_3 \xi_2^D) \quad (4)$$

$$D_{12} = \frac{h^3}{12} (U_4 - U_3 \xi_2^D) \quad (5)$$

$$D_{66} = \frac{h^3}{12} (U_5 - U_3 \xi_2^D) \quad (6)$$

$$D_{16} = \frac{h^3}{24} U_2 \xi_3^D \quad (7)$$

$$D_{26} = \frac{h^3}{24} U_2 \xi_3^D \quad (8)$$

$$(9)$$

2.2 Feasible stacking sequences

We are interested here in conventional laminates of fiber orientations $[0^\circ/45^\circ/-45^\circ/90^\circ]$. These are quite classical orientation used in many references. It should be noted however that use of other prescribed orientations

is often reported to lead to better results in terms of optimization, see for instance [25]. We used the following common feasibility rules that both come from mechanical properties and manufacturability constraints:

- Symmetric laminates. This ensures that the B tensor vanishes. Note that there exist laminates with $B = 0$ that are not symmetric.
- Balanced laminates. The number of 45° layers is equal to the number of -45° layers. This makes the A_{16} and A_{26} terms of the A tensor vanish.
- Contiguity rule. No more than 4 successive layers of the same orientation.
- Disorientation rule. No more than 45° of angle difference between 2 successive layers. In particular the sequence $[45^\circ / -45^\circ]$ is not allowed although many references in the literature on composite design allow it.
- Percentages rule. Each orientation should be represented in the laminate. We took 8% as a minimum percentage of each orientation.

Based on these rules, the number of feasible stacking sequences remains relatively low for thin laminates. The number of feasible stacking sequences based on these rules for a 2×10 layers symmetric laminate is for instance 7032. We found numerically that we could very easily exhaust all feasible stacking sequences based on vector-oriented programming language (such as Matlab) up to symmetric laminates of 34 layers (2×17). Our concern here is not in finding such feasible stackings but it should be noted that for thicker laminates this exhaustive search might take excessive memory resources unless proportions are given and a discrete optimization is preferable. However, for relatively thin laminates (such as the ones used for aircraft fuselage or wing) we consider that we have all feasible stacking sequences and that an exact optimization can be performed by listing all the feasible laminates. We depicted Fig. 1 the logarithm of the number of feasible stacking sequences from 8 to 34 plies. This number $N_{feas}(n)$ where n stands for the number of plies can be approximated by

$$N_{feas}(n) = K 1.72^n \quad (10)$$

where $K \simeq 0.12$.

3 Behavior of the critical buckling factor

In this section, we first recall some basic facts on buckling, including the definition of the critical buckling factor for thin composite plates through variational formulation. Based on this definition we show that this

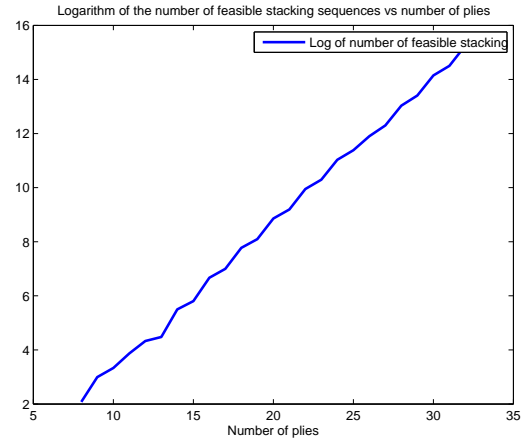


Fig. 1 Logarithm of the number of feasible stacking sequences from 8 to 34 plies

critical buckling factor is concave over bending lamination parameters. We then depict two interesting aspects: firstly, the typical behavior of the critical buckling factor when the stacking sequence varies and secondly the typical behavior of its reciprocal when the loading conditions vary.

3.1 Generalities on buckling

The buckling phenomenon for thin plates and shells has been extensively studied since the beginning of the 20th century. The first rigorous equations for large deflections of thin plates were written down by von Kármán in 1910. In their first derivation for isotropic homogeneous structures, these equations were a system of two nonlinear partial differential equations of order four. As outlined in [3], the mathematical analysis used to solve these equations involved development of bifurcation theory, as it can be found in [8], [29] and [4]. A very brief introduction to bifurcation theory not specifically devoted to buckling can be found in [38]. The major idea is that bifurcation points of the nonlinear partial differential equation's (or stability points where the trivial solution $w = 0$ ceases to be unique) are to be found amongst the points where the linearized operator is not invertible thanks to implicit functions theorem. The topological Leray-Schauder degree theory offers the other way around. Namely, the points where the linearized operator is not invertible (precisely the eigenelements of the linearized operator) are actually bifurcation points of the original nonlinear pde system. We will not delve into the mathematical theory but this brief explanation means that buckling is a nonlinear phenomenon that is often partially solved through a linear eigenvalue problem. It is worth noting

that the linearized buckling can not describe the behavior of the material after buckling, it only predicts the onset of buckling. Being an eigenfunction, the buckled transverse displacement is known up to a multiplicative constant, which means that no maximal transverse displacement can be computed through linear buckling. To study the behavior of plates or shells after buckling one should go to nonlinear analysis, the first work on post-buckling can be found in the seminal paper [28]. Our concern here is on the prediction of buckling, we will therefore study buckling of laminated composite plates into the framework of linear buckling. We will only consider symmetric laminates, which means that the B tensor vanishes and hence that there is no coupling between in-plane and out-of-plane behaviors. Under Kirchhoff hypothesis, one can show (see [43]) that the equation for buckling of a simply supported composite plate leads to the following eigenvalue problem. The *critical buckling factor* is defined as the smallest positive eigenvalue λ_1 of

$$D_{11} \frac{\partial^4 w}{\partial x^4} + D_{22} \frac{\partial^4 w}{\partial y^4} + 2(D_{12} + 2D_{66}) \frac{\partial^4 w}{\partial x^2 \partial y^2} + 4D_{16} \frac{\partial^4 w}{\partial x^3 \partial y} + 4D_{26} \frac{\partial^4 w}{\partial y^3 \partial x} = \lambda_1 (N_x \frac{\partial^2 w}{\partial x^2} + N_y \frac{\partial^2 w}{\partial y^2} + N_{xy} \frac{\partial^2 w}{\partial x \partial y}) \quad (11)$$

where w is the transverse displacement, with $w = 0$ on $\partial\Omega$ and $\Delta w = 0$ on $\partial\Omega$. N_x , N_y and N_{xy} are the loads per unit length respectively for longitudinal, lateral and shear loading, and equivalently the *critical buckling load* N_{cr} is defined as $N_{cr} = \lambda_{cr}(N_x, N_y, N_{xy})$. Note that equation (11) is valid for any geometry Ω . For the numerical experiments in this article, we only focus on rectangular plates but, in general, we can already see that buckling essentially depends on three different types of parameters :

- Ω : the domain where the buckling equation (11) is defined. Dependence of eigenvalue problems to the geometry is quite complicated. For rectangular plates $\Omega = [0, a] \times [0, b]$, the eigenvalues depend only on the aspect ratio $\frac{a}{b}$.
- D tensor: the idealized buckling problem studied in shape optimization (in [5] for instance) only defines bi-Laplacian and Laplacian operators. This corresponds to buckling for isotropic homogeneous material under bi-axial compression of the same magnitude ($N_x = N_y < 0$). For composite, the D tensor makes the buckling equation somewhat more complex since it weights the different derivatives and we clearly see that the D_{16} and D_{26} (bending-twisting terms) are not part of the bi-laplacian.

- $N = (N_x, N_y, N_{xy})$: the loading conditions. When $N_{xy} = 0$ and $N_x = N_y < 0$, note that the right-hand differential operator boils down to a Laplacian.

Buckling problems of this type can be solved exactly in a few cases with simple geometry (rectangles, disk,...) and simple operators (bi-Laplacian that corresponds to orthotropy, Laplacian that corresponds to uniform bi-axial compression with no shear), many closed-form expressions can be found in [30]. In the orthotropic case, where $D_{16} = D_{26} = 0$, buckling of a rectangular composite plate of dimension $[0, a] \times [0, b]$, under bi-axial loading (no shear), the critical buckling factor is

$$\lambda_1 = \min_{m, n \in \mathbb{N}^2} \frac{\pi^2 (D_{11}m^4 + 2(D_{12} + 2D_{66})m^2n^2R^2 + D_{22}n^4R^4)}{a^2(N_xm^2 + N_y n^2R^2)} \quad (12)$$

where $R = a/b$ is the aspect ratio and n (resp. m) is the number of half-waves of the transverse displacement along x direction (resp. y direction). When no closed-form expression can be derived, more complex geometry, non-orthotropic laminates, shear loading, approximation methods are to be used. Amongst the classical methods, we have

- Rayleigh-Ritz method: historically, this was the first method developed to tackle with eigenvalue problem arising in vibration and buckling. This yields to solve a generalized eigenvalue problem over a finite-dimensional space which is the span of natural eigenfunctions for a simple operator, e.g $\sin(\frac{i\pi x}{a}) \sin(\frac{j\pi y}{b})$ for a rectangular plate. The idea is therefore to write the variational characterization of eigenvalue as an optimization problem solved in this finite-dimensional space. The Rayleigh-Ritz method can be thought as a perturbation method (see Appendix B). General introduction can be found in [10], [2] and [43] for composite buckling,
- Finite strip method (see [43]),
- Finite elements method.

In general, the approximation space of finite dimension \mathcal{V}_h is included in the \mathcal{V} Hilbert space where the solution w belongs to (conformal approximation). Under this usual property, the exact eigenvalues can be shown to be approximated by above through these different approximation methods. In this paper, most of the numerical computations were done with a Rayleigh-Ritz method.

A few basic facts can be noted in Eq. (12) regarding the dependence of λ_1 with respect to stacking sequence and loading conditions.

- For fixed loading conditions, critical buckling factor is concave over the D tensor variables, being the minimum of concave functions (linear). We will see in the sequel that this can be established rigorously in the general non-orthotropic case, for any loading and any geometry Ω .
- For fixed stacking sequence, hence fixed D tensor, the reciprocal of the critical buckling factor is piecewise linear. We will see that numerically it seems to be a good approximation for non-orthotropic laminates under bi-axial loading.
- For fixed loading conditions, the critical buckling factor is piecewise linear on D hence on lamination parameters. In the general case (combined loading conditions) this does not seem to be still valid, however, simple piecewise quadratic models over lamination parameters are shown to be very accurate to predict the critical buckling factor.
- Define formally a critical buckling factor function

$$\begin{aligned} \lambda_{cr} : S_3(\mathbb{R})^{++} \times \mathbb{R}^3 &\mapsto \mathbb{R}^+ \\ (D, N_x, N_y, N_{xy}) &\mapsto \lambda_1 = \lambda_{cr}(D, N_x, N_y, N_{xy}) \end{aligned} \quad (13)$$

where D is the out-of-plane (symmetric positive definite) tensor in $S_3(\mathbb{R})^{++}$ (convex cone of symmetric definite positive tensors) and $N = (N_x, N_y, N_{xy})$ the loading conditions. We see that in the orthotropic case, λ_{cr} does have some partial homogeneity properties (e.g $\lambda_{cr}(\kappa N) = \kappa^{-1} \lambda_{cr}(N)$). Most of these properties are still valid in the general case (non-orthotropic and combined loading), this is showed in the sequel.

3.2 Characterization of the critical buckling factor and properties

In most cases, complex geometry, shear loading, non-orthotropic laminate, no closed-form expression can be derived. One way to derive some properties of the critical buckling factor λ_1 is through variational formulation. Let us define some notations for sake of clarity

- $\mathcal{V} = W_0^{2,2}(\Omega)$, the Hilbert space of feasible displacement satisfying the boundary conditions (clamped)¹.

¹ For simply supported boundary conditions, the variational formulation remains the same. The main difference is that the boundary condition $\Delta u = 0$ can not be satisfied in the Hilbert space but is imposed in the variational formulation. However, a posteriori, solution u is in $W_0^{2,4}(\Omega)$ and the trace of the Laplacian can be defined.

- $\mathcal{H} = W_0^{2,1}(\Omega)$. Note that a key property is that $\mathcal{V} \hookrightarrow \mathcal{H}$ and this embedding is continuous and compact. This ensures that the spectrum is countable. Moreover \mathcal{V} is dense in \mathcal{H} .
- $a_D : \mathcal{V} \times \mathcal{V} \mapsto \mathbb{R}^+$ a continuous symmetric bilinear coercive form where D is an element of $S_3(\mathbb{R})^{++}$
- $b_N : \mathcal{H} \times \mathcal{H} \mapsto \mathbb{R}$ a continuous symmetric bilinear form that need not be positive with $N = (N_x, N_y, N_{xy})$. A basic assumption to ensure existence of (realistic) positive buckling eigenvalues is that there exists $w \in \mathcal{H}$ such that $b_N(w, w) \geq 0$ (see Appendix C).

In the case of buckling of composite laminate these bilinear forms are

$$\begin{aligned} a_D(u, v) = & \iint_{\Omega} D_{11} \frac{\partial^2 u}{\partial x^2} \frac{\partial^2 v}{\partial x^2} + D_{22} \frac{\partial^2 u}{\partial y^2} \frac{\partial^2 v}{\partial y^2} + 2(D_{12} + D_{66}) \\ & \frac{\partial^2 u}{\partial x \partial y} \frac{\partial^2 v}{\partial x \partial y} + 4D_{16} \frac{\partial^2 u}{\partial x^2} \frac{\partial^2 v}{\partial x \partial y} + 4D_{26} \frac{\partial^2 u}{\partial y^2} \frac{\partial^2 v}{\partial x \partial y} dx dy \end{aligned} \quad (14)$$

and

$$\begin{aligned} b_N(u, v) = & - \iint_{\Omega} N_x \frac{\partial u}{\partial x} \frac{\partial v}{\partial x} + N_y \frac{\partial u}{\partial y} \frac{\partial v}{\partial y} + \frac{N_{xy}}{2} \left(\frac{\partial u}{\partial x} \frac{\partial v}{\partial y} + \frac{\partial u}{\partial y} \frac{\partial v}{\partial x} \right) dx dy \end{aligned} \quad (15)$$

The coercitivity of a_D simply follows from Poincaré's inequality applied to each component of the gradient of u and from the positivity of the D tensor. We now have the following characterization of λ_1 , known as the Courant-Fisher characterization²

$$\lambda_{cr}(D, N_x, N_y, N_{xy}) = \lambda_1 = \min_{w \in \mathcal{V} \setminus \{0\}} \frac{a_D(w, w)}{|b_N(w, w)|} \quad (16)$$

Let's first recall a result from [35] that states that λ_{cr} is continuous over D, N_x, N_y, N_{xy} . However differentiability can not be established, indeed, what is showed in [35] is that λ_{cr} is differentiable whenever it is a simple eigenvalue, in case it is a multiple eigenvalue only directional differentiability can be established.

We can use (16) to derive some homogeneity properties. Let $\kappa > 0$ and $D \in S_3(\mathbb{R})^{++}$, $N = (N_x, N_y, N_{xy})$, for any $w \in \mathcal{V}$

$$a_{\kappa D}(w, w) = \kappa a_D(w, w) \quad (17)$$

² Note that the original Courant-Fisher characterization does not use absolute value over the bilinear form b_N . This convention, used also in [35] does not change the value of λ_{cr} for loading conditions that 'really' give rise to buckling, since in that case λ_{cr} is attained over a positive eigenfunction a_D being coercive (see Appendix C). It simply allows to define λ_{cr} everywhere in \mathbb{R}^3 .

and

$$|b_{\kappa N}| = \kappa |b_N(w, w)| \quad (18)$$

Taking the infimum over \mathcal{V} , we get

$$\lambda_{cr}(\kappa D, N) = \kappa \lambda_{cr}(D, N) \quad (19)$$

and

$$\lambda_{cr}(D, \kappa N) = \frac{1}{\kappa} \lambda_{cr}(D, N) \quad (20)$$

(19) and (20) mean that λ_{cr} is *homogeneous of degree 1* over D and *homogeneous of degree -1* over N . Applying Euler identity theorem (see Appendix A) to (19) and (20) whenever λ_{cr} is differentiable gives

$$\sum_{i=1}^6 D_i \frac{\partial \lambda_{cr}}{\partial D_i} = \lambda_{cr} \quad (21)$$

$$\sum_{i=1}^3 N_i \frac{\partial \lambda_{cr}}{\partial N_i} = -\lambda_{cr}. \quad (22)$$

These equations can be used within an optimization process to save sensitivity analysis computations. Note that by simply rewriting (20) in terms of the reciprocal of the critical buckling factor

$$\frac{1}{\lambda_{cr}(D, \kappa N)} = \frac{\kappa}{\lambda_{cr}(D, N)} \quad (23)$$

and we see that the reciprocal of λ_{cr} is homogeneous of degree 1, which yields

$$N_x \frac{\partial \frac{1}{\lambda_{cr}}}{\partial N_x} + N_y \frac{\partial \frac{1}{\lambda_{cr}}}{\partial N_y} + N_{xy} \frac{\partial \frac{1}{\lambda_{cr}}}{\partial N_{xy}} = \frac{1}{\lambda_{cr}}. \quad (24)$$

Note any of equations (21), (22) and (24) can be used to directly derive an exact expression of the reciprocal of the critical buckling factor whenever the partial derivatives are simple (e.g piecewise constant). It should be emphasized however that these equations are not globally valid in the whole domain since the derivatives of λ_{cr} do not exist everywhere. We will see in the sequel that these equations are valid piecewise, since λ_{cr} is differentiable over connected regions that can be easily described.

The homogeneity of the critical buckling factor, which was already noticed, for instance with respect to the loading conditions in [18], can of course be used to reduce the size of the regression problem. One way to use it would be to build an approximation model over the sphere of radius $\{||N|| = K\}$ and use for instance the spherical coordinates (θ, ϕ) as approximation variables.

However doing so we would definitely reduce the dimension but we are likely to miss some simple dependence of λ_{cr} over the natural variables N . We can also observe that if we consider the critical buckling factor defined over the panel thickness h and the lamination parameters ξ_D instead of being defined over the D tensor, we get

$$\lambda_{cr}(\kappa h) = \kappa^3 \lambda_{cr}(h) \quad (25)$$

This equation means that we can get rid of panel thickness h and only focus on lamination parameters. Finally, we can also observe that for the specific case of rectangular plates, we have by applying the change of coordinates $x' = \kappa x$ and $y' = \kappa y$

$$\lambda_{cr}(\kappa a, \kappa b) = \frac{1}{\kappa^2} \lambda_{cr}(a, b) \quad (26)$$

and the corresponding Euler identity

$$a \frac{\partial \lambda_{cr}}{\partial a} + b \frac{\partial \lambda_{cr}}{\partial b} = 2 \lambda_{cr} \quad (27)$$

Note that Eq. (26) in reality can be derived for any domain Ω . Following the derivation ³ in [21] where this formula is stated for the eigenvalues of the Laplacian, we have for any domain Ω and $\kappa > 0$

$$\lambda_{cr}(\kappa \Omega) = \frac{\lambda_{cr}(\Omega)}{\kappa^2}. \quad (28)$$

3.3 Concavity of the buckling factor over lamination parameters

We now turn on the concavity of λ_{cr} . To show that it is concave over the ξ_D , we first show that it is concave over D , concavity being preserved by pre-composition by an affine function (with h fixed), concavity over ξ_D will be ensured.

In this paragraph, the loading conditions remain fixed, we therefore skip them when writing the dependence of λ_{cr} . We want to show that λ_{cr} is concave over $S_3(\mathbb{R})^{++}$. Let $\alpha > 0$, consider the upper level set $D_\alpha = \{D \in S_3(\mathbb{R})^{++} \text{ s.t. } \lambda_{cr} \geq \alpha\}$. Let $D^{(1)}$ and $D^{(2)}$ in D_α and $\theta \in (0, 1)$, let denote $D^{(\theta)} = \theta D^{(1)} + (1 - \theta) D^{(2)}$. $S_3(\mathbb{R})^{++}$ being convex, $D^{(\theta)}$ is clearly a symmetric positive definite tensor and consider now the bilinear form

³ by noting that $H_\kappa \circ \Delta^2 = \kappa^4 \Delta^2 \circ H_\kappa$ and $H_\kappa \circ \Delta = \kappa^2 \Delta \circ H_\kappa$ where $H_\kappa v$ is the function defined over $\mathcal{V}(\kappa \Omega)$ such that $H_\kappa v(x) = v(x/\kappa)$. Note that Eq. (26) is homogeneous of order 2 because buckling equation is essentially the diagonalization of a fourth-order operator with respect to a second-order operator. For pure fourth-order problems (vibrations), we would get homogeneity of order 4

$a_{D(\theta)}$. It is clearly continuous, symmetric and coercive. Let $w \in \mathcal{V}$ we then have

$$a_{D(\theta)}(w, w) = \theta a_{D(1)}(w, w) + (1 - \theta) a_{D(2)}(w, w) \quad (29)$$

hence

$$\frac{a_{D(\theta)}(w, w)}{b_N(w, w)} = \theta \frac{a_{D(1)}(w, w)}{b_N(w, w)} + (1 - \theta) \frac{a_{D(2)}(w, w)}{b_N(w, w)} \quad (30)$$

Since $D^{(1)}$ and $D^{(2)}$ are in D_α , for all $w \in \mathcal{V}$

$$\frac{a_{D(1)}(w, w)}{b_N(w, w)} \geq \alpha \quad (31)$$

and

$$\frac{a_{D(2)}(w, w)}{b_N(w, w)} \geq \alpha \quad (32)$$

hence for all $w \in \mathcal{V}$

$$\frac{a_{D(\theta)}(w, w)}{b_N(w, w)} \geq \alpha \quad (33)$$

and $D^{(\theta)}$ is in D_α . This implies that λ_{cr} is quasiconcave, since its upper level sets D_α are convex. Being also homogeneous of degree 1, it is concave (see Appendix A). Note that strict concavity cannot be ensured, this follows obviously from equation (12) where we see that in the vicinity of $(\xi_D^1, \xi_D^2, 0)$, λ_{cr} is a minimum of linear functions, hence at a point where λ_{cr} is differentiable, there exists a neighborhood where λ_{cr} is linear over (ξ_D^1, ξ_D^2) and cannot be strictly concave. Another quick way to see that is to note that, in case λ_{cr} is twice continuously differentiable over D , Euler identity for the homogeneity of order 0 of each partial derivative of λ_{cr} w.r.t to D_j yields

$$\forall j = 1 \dots 6 \quad \sum_{i=1}^6 D_i \frac{\partial^2 \lambda_{cr}}{\partial D_j \partial D_i} = 0 \quad (34)$$

Equation (34) simply means that D belongs to the kernel of the Hessian $H\lambda_{cr}(D)$ of λ_{cr} at D and hence $H\lambda_{cr}(D)$ is not definite.

Using the following definition of the reciprocal $1/\lambda_{cr}(N)$

$$1/\lambda_{cr}(N) = \max_{w \in \mathcal{V}} \frac{|b_N(w, w)|}{a_D(w, w)} \quad (35)$$

together with the following lower level sets $N_\alpha = \{N \in \mathbb{R}^3 \text{ s.t. } 1/\lambda_{cr}(N) \leq \alpha\}$ and the triangular inequality leads to the quasiconvexity of $1/\lambda_{cr}(N)$ over N . Being homogeneous of degree 1 it is convex. Strict convexity of $1/\lambda_{cr}(N)$ cannot be ensured the same way as the strict concavity of $\lambda_{cr}(\xi_D)$.

Table 1 Graphite/Epoxy material characteristics

Characteristics	Graphite/Epoxy
E_1 Longitudinal modulus	112 GPa
E_2 Transverse modulus	8.2 GPa
G_{12} Shear modulus	4.5 GPa
t Elementary ply thickness	0.26 mm

3.4 Influence of the stacking sequence

We focus in this section on the behavior of the critical buckling factor λ_{cr} when the loading N is fixed and when the stacking sequence of the plate laminate varies. We use lamination parameters ξ_D to assess this behavior. We focused here on lamination parameters of conventional laminates $[0^\circ/45^\circ/-45^\circ/90^\circ]$, in that case $\xi_D^4 = 0$. We then restrict our study to the influence of $(\xi_D^1, \xi_D^2, \xi_D^3)$ over the feasible domain described in [9], [22] and [23]

$$2|\xi_D^1| - \xi_D^2 - 1 \leq 0 \quad (36)$$

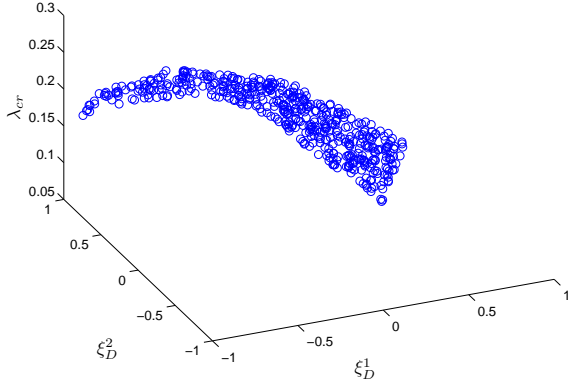
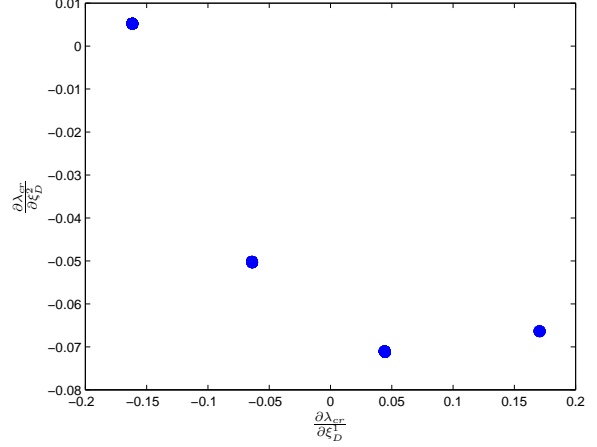
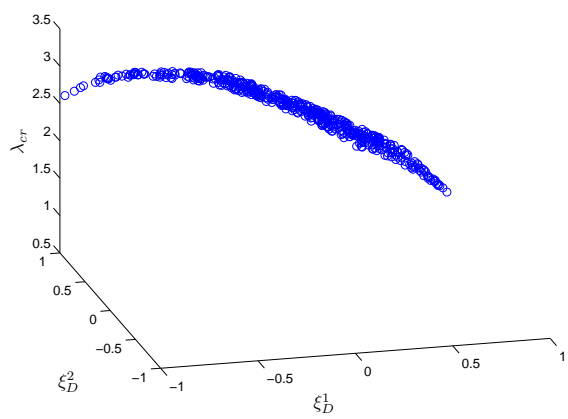
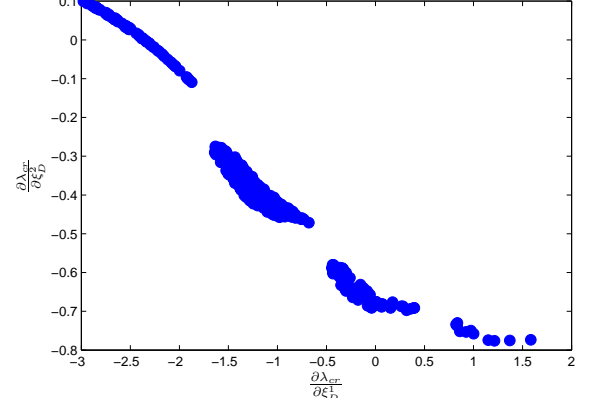
and

$$2|\xi_D^3| + \xi_D^2 - 1 \leq 0 \quad (37)$$

Note that it is a convex domain. The triangle in $[-1, 1]^2$ that Eq. (36) will be referred to as *Miki's triangle* (with $\xi_D^3 = 0$) and the polyhedron in $[-1, 1]^3$ defined both by Eq. (36) and Eq. (37) will be referred to as *Miki's tetrahedron*. The main interest of the compatibility equations described in [22] is that they provide a convex feasible set for $\xi_D \in [-1, 1]^3$ for given in-plane lamination parameters ξ_A (or equivalently proportions of fiber orientation). In an optimization process, this offers a way to ensure compatibility in a continuous way between in-plane properties (A tensor) and out-of-plane properties (D tensor). In the sequel we study the behavior of λ_{cr} all over its definition domain with no regards to proportions, but we should keep in mind that in practice, the out-of-plane lamination parameters are related to proportions (or equivalently ξ_A). Note that most of the computations done in this article were based on a Rayleigh-Ritz method (see Appendix B) with $N = 20 \times 20$ basis functions over a rectangular plate of dimensions $a = 650\text{mm}$ and $b = 250\text{mm}$, we chose a classical Graphite/Epoxy whose characteristics are given Tab. 1.

3.4.1 Behavior of λ_{cr} for orthotropic laminates under combined loadings and pure shear

For uni-axial and bi-axial compressive loadings, a closed-form equation is given by Eq. (12). For fixed loading, it follows that λ_{cr} is piecewise linear over tensor D terms

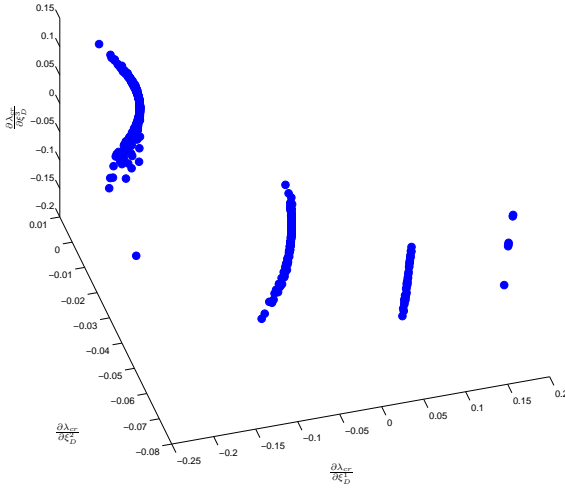
λ_{cr} over Miki's triangle for orthotropic laminates for combined loading(a) Piecewise dependence of λ_{cr} over ξ_D^1 and ξ_D^2 on Miki's triangle for combined loading $N_x = -50N.mm^{-1}$, $N_y = -20N.mm^{-1}$ and $N_{xy} = 20N.mm^{-1}$ Phase portrait of λ_{cr} for orthotropic laminate for combined loading(b) Phase portrait associated to the couple ξ_D^1, ξ_D^2 for combined loading. Each point is the associated partial derivatives λ_{cr} over Miki's triangle for orthotropic laminates for pure shear(c) Piecewise dependence of λ_{cr} over ξ_D^1 and ξ_D^2 on Miki's triangle for pure shear loading $N_x = 0N.mm^{-1}$, $N_y = 20N.mm^{-1}$ and $N_{xy} = 20N.mm^{-1}$ Phase portrait of λ_{cr} for orthotropic laminate for pure shear loading(d) Phase portrait associated to the couple ξ_D^1, ξ_D^2 for pure shear loading. Each point is the associated partial derivatives**Fig. 2** Results for orthotropic laminates under combined loading and pure shear loading

and therefore piecewise affine over ξ_D . For combined loadings (including shear) or pure shear loading, no closed form expression can be derived. The main reason for this is that the $\frac{\partial^2 w}{\partial x \partial y}$ term prevents from using the classical techniques as a double sine series (see [34]). Correction formulas were given (see for instance [45]), but all of them were approximation expressions based on simplified assumption (infinite length plate for instance) and there is no evidence at the time being that

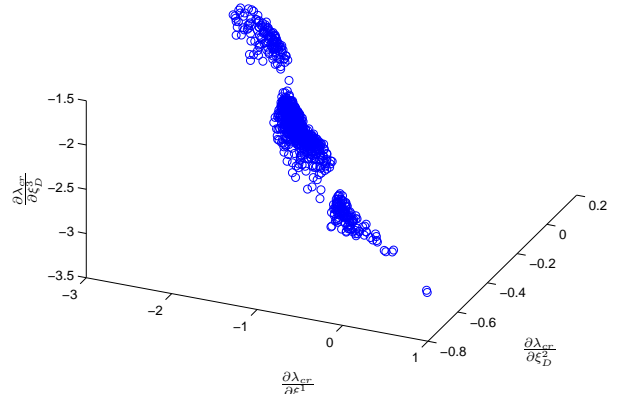
- for arbitrary loading (combined loading, pure shear), λ_{cr} is still piecewise affine over ξ_D for orthotropic laminate
- for arbitrary loading, λ_{cr} can be defined in a piecewise manner for non-orthotropic laminates.

In the sequel, we show numerically that λ_{cr} seems to be piecewise affine over ξ_D for combined loading where shear is not very high. However, for pure shear loading, we observed that λ_{cr} can still be defined in a piecewise manner but each part of the function seems to be more complex than affine functions. The most important fact shown here is that λ_{cr} behaves in a piecewise manner and a good approximation technique should be able to detect these different regions or so-called modes and build an approximator for each region.

To assess the evolution of λ_{cr} , we sample uniformly Miki's triangle for ξ_D^1, ξ_D^2 and compute for each couple of lamination parameters its associated λ_{cr} . The loading is taken as combined loading with shear and we also compute the associated sensitivities $\frac{\partial \lambda_{cr}}{\partial \xi_D^1}$ and $\frac{\partial \lambda_{cr}}{\partial \xi_D^2}$ and

Phase portrait of λ_{cr} for varying ξ_D 

(a) Phase portrait associated to the couple ξ_D^1, ξ_D^2 for combined loading $N_x = -50 \text{ N.mm}^{-1}$, $N_y = -20 \text{ N.mm}^{-1}$ and shear loading $N_x = 0 \text{ N.mm}^{-1}$, $N_y = 0 \text{ N.mm}^{-1}$ and $N_{xy} = 20 \text{ N.mm}^{-1}$. Each point is the associated partial derivatives

Phase portrait of λ_{cr} for non-orthotropic laminates for pure shear loading

(b) Phase portrait associated to the couple ξ_D^1, ξ_D^2 for pure shear loading $N_x = 0 \text{ N.mm}^{-1}$, $N_y = 0 \text{ N.mm}^{-1}$ and $N_{xy} = 20 \text{ N.mm}^{-1}$. Each point is the associated partial derivatives

Fig. 3 Results for non-orthotropic laminates under combined loading and pure shear loading

plot the phase portrait: for each couple we associate a point of the gradient space.

The different plots depicted Fig. 2 were obtained for two different loading conditions

- Combined loading: $N_x = -50 \text{ N.mm}^{-1}$, $N_y = -20 \text{ N.mm}^{-1}$, $N_{xy} = 20 \text{ N.mm}^{-1}$
- Pure shear loading: $N_x = 0 \text{ N.mm}^{-1}$, $N_y = 0 \text{ N.mm}^{-1}$, $N_{xy} = 20 \text{ N.mm}^{-1}$.

For each loading case, we generated 800 couples (ξ_D^1, ξ_D^2) uniformly distributed over Miki's triangle. We depicted the behavior of λ_{cr} Fig. 2 a) and 2 c). We can observe that for the first loading case, we clearly see the piecewise dependence of λ_{cr} over (ξ_D^1, ξ_D^2) , as in the bi-axial compression case of Eq. (12), λ_{cr} seems still defined as the minimum of hyperplanes, making the overall function simply defined over a sole hyperplane but not differentiable at the boundaries between hyperplanes. It is worth noting that directional differentiability seems still valid as it is proved in [35]. For this loading case, λ_{cr} seems to be still defined as piecewise linear, this is numerically ensured by the phase portrait Fig. 2 b), where we see all the 800 points shrink down to only 4 different points, which means over each region, λ_{cr} is linear or very close to be linear. For the pure shear loading case, this dependence does not seem to hold, indeed, the regions are not as clearly defined as in the combined loading. The phase portrait shows 4 different

regions disconnected, which again means that λ_{cr} can be defined in a piecewise manner, though its behavior over each region seems more complicated than linear.

3.4.2 Behavior of λ_{cr} for non-orthotropic laminates under combined loadings and pure shear

We also depicted the phase portrait for non-orthotropic laminates by making the ξ_D varying in the Miki's tetrahedron for the same loadings. We observe in both cases that the phase portrait has the same structure that is to say 4 disconnected components. However, the dispersion of these clusters is quite different for the two loadings (cf. Fig. 3). In the first case, for combined loading, we observe a low variance over the two first dimensions $(\frac{\partial \lambda_{cr}}{\partial \xi_D^1}, \frac{\partial \lambda_{cr}}{\partial \xi_D^2})$ and bigger variations for the last dimension $(\frac{\partial \lambda_{cr}}{\partial \xi_D^3})$, this would naturally indicate that λ_{cr} is close to depend linearly over the two first dimensions and that it depends in a more complex manner over the last dimension. In case of pure shear loading, the dependence is much more complex, it does not seem that there is a dimension that has a bigger influence than the others. However, the main observation that we can make is that in all cases, λ_{cr} seems to depend in a piecewise manner and that the function is likely to be well approximated when taking advantage of this structure.

3.5 Influence of the loading conditions

In this section, we are interested in the behavior of the λ_{cr} for fixed stacking sequence $([-45/-45/0/45/90/-45/0]_S)$ when the loading conditions vary. In most cases, when loading conditions vary, the reciprocal of λ_{cr} was found to be more easier to depict and interpret. This can be easily seen again in the general formula (16) where all the stacking sequence dependence appear in the numerator and all the loading conditions appear in the denominator. Furthermore, it also follows from both theoretical and computational considerations. Indeed, for instance in [35], the authors do not study directly λ_{cr} but first use its reciprocal to show it is continuous and differentiable whenever it is a simple eigenvalue. Numerically, it is preferable to compute the reciprocal of λ_{cr} that is to find w and the largest κ such that

$$Lw = \kappa Kw \quad (38)$$

where K is the matrix associated to the a_D bilinear form (stiffness material matrix) and L matrix associated to the b_N bilinear form (geometry stiffness matrix) and eventually $\lambda_{cr} = 1/\kappa$. Next, as noted before, in case of the orthotropic formula, we can observe that $1/\lambda_{cr}$ is piecewise linear over $N = (N_x, N_y)$. Regarding computational issues when making the loading conditions vary, it can be noted that for general loading (including shear) the feasible set (i.e the fluxes that gives rise to buckling, this is related to the assumption of positivity of b_N) are not easy to describe. When the loading conditions approach near the boundary, the eigensolver might not converge or exhibit numerical ill-conditioning behavior and λ_{cr} increases very quickly and behaves like an hyperbola (cf. Fig. 4).

4 Original strategy to approximate the critical buckling factor

In a recent paper [7], the authors developed a strategy to approximate discontinuous or derivative discontinuous functions by means of clustering of the learning basis into regions where the function to be approximated is expected to be continuous or at least more simple. It strongly relies on the EM algorithm (Expectation-Maximization), which is a classical algorithm in statistics to solve maximum-likelihood problem, such as density estimation. In this case, the learning data (input and output) is modeled as a finite mixture of multivariate Gaussians. The EM algorithm is first used to estimate the mixtures parameters (weights of each mixture component, means and variance-covariance matrices of each Gaussian component), a clustering is performed on

the data (by means of Maximum A Posteriori), a local expert is built over each region, marginal densities are then derived from the finite mixture parameters and a final approximation model is built as

$$f(x) = \sum_{i=1}^K \mathbb{P}(\kappa = i|X = x) f_i(x) \quad (39)$$

where K is the number of Gaussian components, $\mathbb{P}(\kappa = i|X = x)$ is the probability to lie in cluster i knowing that $X = x$ and f_i is the local expert built on cluster i . Eq. (39) leads to two different approximation models depending on the computation of $\mathbb{P}(\kappa = i|X = x)$. When choosing the Gaussian laws to compute this quantity, Eq. (39) leads to a smooth model that smoothly recombine different local experts. If $\mathcal{P}(i|X = x)$ is computed as characteristic functions of clusters (being equal to 0 or 1) this leads to a discontinuous approximation model. Depending on the application, the smooth recombination can be used for instance in a gradient-based method, while if derivative free optimization algorithms are to be used, the discontinuous (or hard) recombination is preferable whenever it gives a better accuracy. Based on former numerical experiments where this strategy showed to be adequate to approximate discontinuous or derivative discontinuous functions and on the behavior of λ_{cr} as described in the former sections, we want to apply this strategy to the approximation of λ_{cr} with a specified type of local experts f_i (linear, polynomial and rational).

4.1 Piecewise polynomial approximation in lamination space

The behavior of $\lambda_{cr}(\xi_D^1, \xi_D^2)$ for orthotropic laminates for combined loading (with low shear) seems to be piecewise linear (or close to be linear). We then want to approximate λ_{cr} based on a mixture of linear experts (referred to as MOL). The number of clusters is chosen through a range of potential clusters by minimizing the generalization error for the mixture of linear experts. We depicted Fig. 5 the result of the EM clustering for 4 clusters on the orthotropic data for combined loading. We see that the hyperplanes are correctly detected through the clustering.

For pure shear and non-orthotropic laminates, the phase portraits showed that the linear dependence does not hold, however λ_{cr} does not seem to behave in a very complicated way over each cluster. We then build an approximation of λ_{cr} on the basis of a mixture of quadratic models (MOQ).

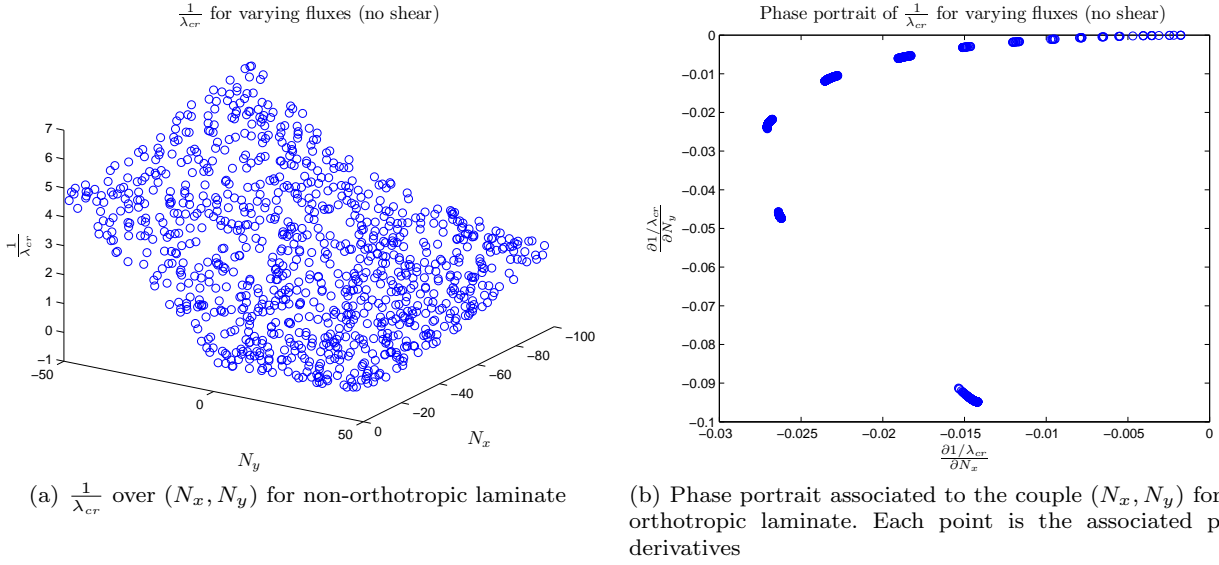


Fig. 4 Results for reciprocal of the buckling critical load for varying loading conditions $N_{xy} = 0 \text{ N.mm}^{-1}$ for a fixed non-orthotropic stacking sequence

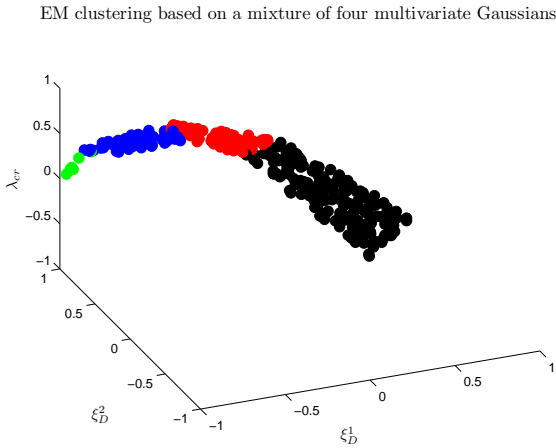


Fig. 5 Automatic clustering (normalized output) for an orthotropic laminate and combined loading

4.2 Piecewise polynomial approximation in forces space

When the loading conditions vary, the dependence of $1/\lambda_{cr}$ seems to get less simple as linear as the plate endures less compression and more complex loading with tension for instance. However for pure compression loading cases, $1/\lambda_{cr}$ is close to be piecewise linear, we then build an approximation model as a mixture of quadratic models since it is expected to be able to handle different situations. It should be noted that if ordinary least squares are used, a linear model can not totally be recovered from a polynomial regression due to the \mathcal{L}_2 minimization that regularizes polynomial coefficients. So more advanced techniques should be used

to build purely linear experts and quadratic experts in different regions (best-subset selection, lasso, least angles regression, compressed sensing).

4.3 Piecewise rational approximation in the general case

Based on the behavior of λ_{cr} with respect to lamination parameters and of $1/\lambda_{cr}$ with respect to loads per unit length N , we want to build an approximation model as a mixture of (quadratic) rational experts

$$f_i(x) = \frac{a_0 + a_1 \xi_D^1 + \dots + a_{n-1} (\xi_D^2)^2 + a_n (\xi_D^3)^2}{b_0 + b_1 N_x + \dots + b_{n-1} N_y^2 + b_n N_{xy}^2} \quad (40)$$

such models will be referred to as Mixture of Rationals (MoR).

4.4 Using directly Rayleigh-Ritz active buckling modes

It is worth noting when using Rayleigh-Ritz method, we usually get an extra information by looking at the eigenvector w_{cr} associated to λ_{cr} . Indeed, it can be written

$$w_{cr} = \sum_{i=1}^N \alpha_i u_i \quad (41)$$

where the u_i 's are the basis functions. These basis functions can be associated to 'natural' modes (that is eigenfunctions of the unperturbed operator or over a more

simple geometry). Suppose we take functions of the type

$$\sin(i\pi x/a) \sin(j\pi y/b). \quad (42)$$

We can associate each eigenvector w_{cr} to the 'closest natural mode' simply by finding the largest (in magnitude) component w_{cr}^{ij} of w_{cr} . However, this process can lead to wrong associated modes, in the case where we have two or more large components in w_{cr} , the numerical approximation is likely to invert the corresponding natural modes. Next, finite element buckling methods do not provide directly such information, since the critical buckled shape (w_{cr}) is defined over local, mesh-dependent, non natural basis functions (\mathcal{P}_1 basis functions...). Post-treatment of the transverse displacement is needed when identifying the corresponding natural mode. This includes tools from mode shape identification well known in vibrations or structural health monitoring like *Modal Assurance Criteria* (MAC). In case modal information is directly provided and can be easily retrieved from the analysis, this offers a natural way to approximate the critical buckling load by approximating mode per mode and building classifiers (linear or more advanced like Support Vector Machine) that give the corresponding natural mode to a new input and hence apply the corresponding approximation model. This can be done for few degrees-of-freedom problems since the regions that separate each natural buckling mode are usually quite simple in the input space. We depicted for instance Fig. 6, the different natural modes when the loading conditions vary both over the loading conditions sphere ($\|N\| = K$) and over spherical angles space (θ, ϕ) , since the active mode does not depend on the norm $\|N\|$. We clearly see Fig. 6 a) that the associated regions are quite simple over the sphere but for the (θ, ϕ) space Fig. 6 b) the regions are not easily separated, which prevents from building accurate classifiers. Even though, this approach seems at first glance easy to apply, there are several drawbacks that prevent from detecting the correct mode. This is the difficult problem of mode tracking well known in structural dynamics and vibrations. For low-dimensional problem (< 3), several phenomena make it difficult to follow one mode when state parameters change: mode crossing, where two modes simply cross each other, mode veering where two nearly-simultaneous modes start to interact and the associated eigenvalues abruptly diverge and finally mode coalescence where two modes shrink down in only one mode. For high-dimensional problems (more than 3 parameters), such our problem, this mode tracking becomes very challenging and even impossible. Furthermore, one has to fix the number of modes to approximate and ensure that all these modes are available

at learning points. Last but not least, the accuracy of the eigenvalues decreases for higher modes, this means that each mode is likely to have a different level of noise all over the input space.

5 Numerical results

We describe the different results obtained with the suggested strategies to approximate λ_{cr} in the different situations.

- For fixed loading: we approximate λ_{cr} first for orthotropic laminates (over ξ_D^1 and ξ_D^2) and then for $[0/45/90]$ laminates (over ξ_D^1 , ξ_D^2 and ξ_D^3) for both combined loading and pure shear loading.
- For a fixed non-orthotropic stacking sequence: we approximate λ_{cr} first for bi-axial loading (over N_x and N_y) and then for combined loading (over N_x , N_y and N_{xy}).
- In the general case when stacking and loading vary: we approximate λ_{cr} over ξ_D^1 , ξ_D^2 , ξ_D^3 , N_x , N_y and N_{xy} .

In all situations, the learning of the approximation models is based on three different bases: learning basis B_A , test basis B_T and validation basis B_V . The learning in itself is directly based on B_A , to compare several approximation model built over B_A , we use B_T to rank them and chose the best one. Finally at the end of this selection process, the generalization error and the other accuracy metrics are computed over the validation basis B_V . Following for instance [14], we have a classical partition of 60 % for B_A , 20 % for B_T and 20 % for B_V . To assess the goodness of the fit, we use several classical metrics, amongst them, we use the *Mean Squared Error* (MSE) and *Lack Of Fit* (LOF) defined as

$$\text{MSE} = \frac{1}{N_V} \sum_{i=1}^{N_V} |\hat{f}(x_i) - y_i|^2 \quad (43)$$

and

$$\text{LOF} = \frac{\text{MSE}}{\text{Var}(\{y_i\}_{i=1 \dots N_V})} \quad (44)$$

where N_V is the number of points in the validation basis, y is the real output function and \hat{f} is the approximation model. The LOF simply divides the MSE by the variance of the output to avoid scaling effect. However the knowledge of only the MSE might not be enough for accuracy evaluation. Indeed, first it does not provide any clue regarding the relative error and more important it is an average over a whole basis and does not give any insight on the distribution of the error. Suppose we have two different approximation models,

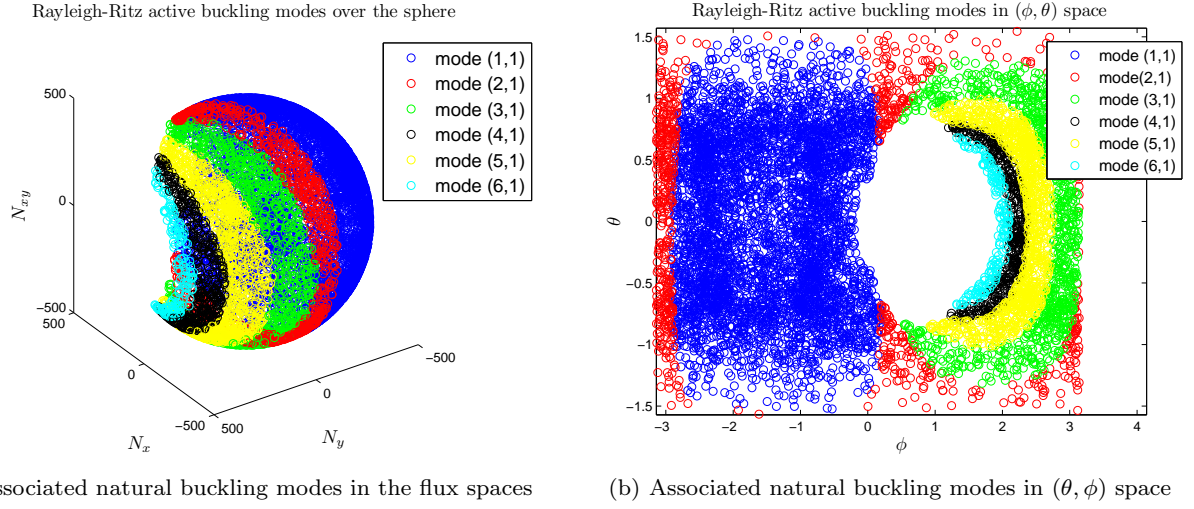


Fig. 6 Active buckling modes found by Rayleigh-Ritz method for different representations

one giving a very good approximation for a majority of points and being very bad for a small amount of points, it will be equivalent in terms of MSE to an approximation model that has a medium error for all points, while the first approximation model is likely to be preferable when used within a population-based algorithm (such as genetic algorithms). This is why, we add several metrics

- \mathcal{L}_1 and \mathcal{L}_∞ errors:
- Mean relative error:

$$\hat{E}_{rel} = \frac{1}{N_V} \sum_{i=1}^{N_V} \frac{|\hat{f}(x_i) - y_i|}{|y_i|}$$

- Mean absolute error:

$$\hat{E}_{abs} = \frac{1}{N_V} \sum_{i=1}^{N_V} |\hat{f}(x_i) - y_i|$$

- Max relative error:

$$E_{rel}^{max} = \max_{i=1 \dots N_V} \frac{|\hat{f}(x_i) - y_i|}{|y_i|}$$

- Max absolute error:

$$E_{abs}^{max} = \max_{i=1 \dots N_V} |\hat{f}(x_i) - y_i|$$

- Cumulative error distribution :
- α -quantiles:

$$Q_\alpha = \frac{\text{Card}\{x_i \in B_V \text{ s.t. } \frac{|\hat{f}(x_i) - y_i|}{\hat{f}(x_i)} \leq \alpha\% \}}{N_V}$$

the proportion of the validation points that are below a relative error of $\alpha\%$.

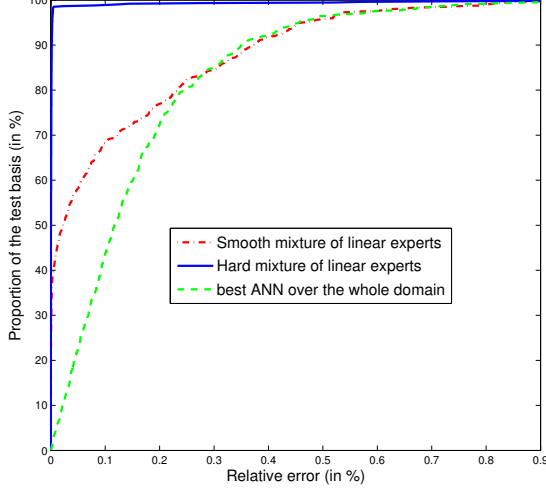
- Quantile curve: curve obtained by making α varying from 0% to $E_{rel}^{max}\%$.

Note also that the number of points used in each case corresponds to the total points used for all bases. To the end of comparison, in each case we compared with a reasonably good artificial neural network built over the whole domain with classical techniques such as cross-validation for the choice of the number of hidden units or backpropagation error for the weight update.

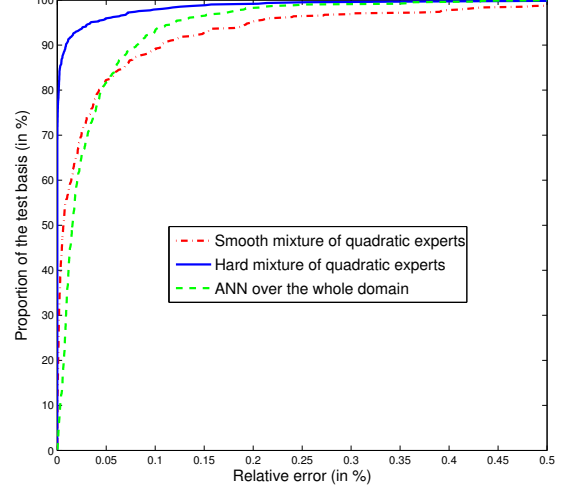
5.1 Approximation models for varying stacking

For the approximation of λ_{cr} for orthotropic laminates, we used $N = 420$ points for the first loading case (combined, $N_x = -50N.mm^{-1}$, $N_y = 20N.mm^{-1}$ and $N_{xy} = 20N.mm^{-1}$) and $N = 430$ points for the second loading case (pure shear). For the combined loading case, a mixture of linear experts was built and for the pure shear case, a mixture of quadratic models. We see Tab. 2 that the mixture model performs equally as the artificial neural network (ANN) for the pure shear and performs better for the combined loading. The quantile curves as described on Fig. 7 a) and 7 b) and the quantiles $Q_{1\%}$ and $Q_{0.1\%}$ (cf Tab. 2) show that the hard recombination of mixture models even when they have the same accuracy in terms of MSE is much more accurate for a large amount of validation points. For combined loading for instance, the quantile curve is very close the y-axis, which means the approximation model is close to be exact except for a few points for which the mixture model gives bad accuracy. This might be due to misclassification, the wrong local expert is called for these few points, while the ANN regularizes the error over the whole domain. The ANN is of a reasonably

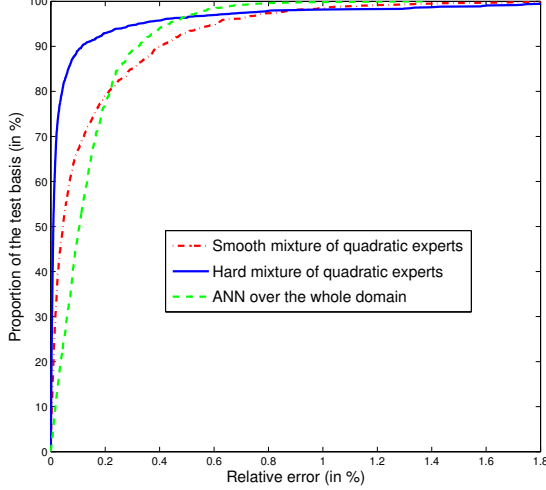
Comparison of cumulative relative error distributions for ANN and mixture of linear expert:



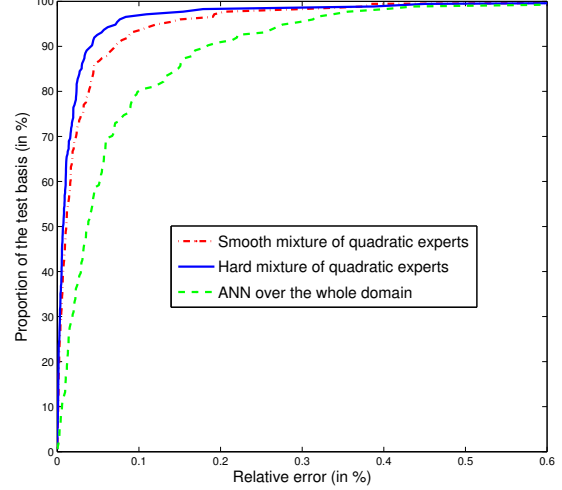
Comparison of cumulative relative error distributions for ANN and mixture of quadratic

(a) Comparison of approximations of λ_{cr} over ξ_D^1 and ξ_D^2 on Miki's triangle for combined loading $N_x = -50N.mm^{-1}$, $N_y = 20N.mm^{-1}$ and $N_{xy} = 20N.mm^{-1}$ (b) Comparison of approximations of λ_{cr} over ξ_D^1 and ξ_D^2 on Miki's triangle for pure shear loading $N_x = 0N.mm^{-1}$, $N_y = 0N.mm^{-1}$ and $N_{xy} = 20N.mm^{-1}$

Comparison of cumulative relative error distributions for ANN and mixture of quadratic



Comparison of cumulative relative error distributions for ANN and mixture of quadratic

(c) Comparison of approximations of λ_{cr} over ξ_D^1 , ξ_D^2 and ξ_D^3 for combined loading $N_x = -50N.mm^{-1}$, $N_y = 20N.mm^{-1}$ and $N_{xy} = 20N.mm^{-1}$ (d) Comparison of approximations of λ_{cr} over ξ_D^1 , ξ_D^2 and ξ_D^3 for pure shear loading $N_x = 0N.mm^{-1}$, $N_y = 0N.mm^{-1}$ and $N_{xy} = 20N.mm^{-1}$ **Fig. 7** Quantile curves for orthotropic and non-orthotropic laminates under combined loading and pure shear loading

good accuracy over all validation points but can not achieve very high accuracy even for a small amount of validation points. Regarding the relative error measures, the mixture models always perform better than ANN.

In the case of non-orthotropic laminates, $N = 853$ points were used for combined loading and $N = 768$ points in the case of pure shear loading. Results are in Tab. 3, again we observe the same behavior (see Fig. 7 c) and

7 d)), the mixture models are by far better in terms of relative error while the MSE show the same tendency. The quantile curves clearly show that the hard recombination of mixture models is better for a majority of points. Regarding the smooth recombination, no clear conclusion can be drawn since it performs better than ANN for pure shear loading and it is less accurate for combined loading.

Table 2 Results for the approximation of λ_{cr} for orthotropic laminates for combined loading and pure shear loading

Loading Type	Combined loading		Pure shear loading	
	MOL	ANN	MOQ	ANN
MSE	$8.5 \cdot 10^{-8}$	$7.8 \cdot 10^{-7}$	$2.1 \cdot 10^{-6}$	$1.7 \cdot 10^{-6}$
LOF(%)	$9.1 \cdot 10^{-4}$	$8.5 \cdot 10^{-3}$	$8.5 \cdot 10^{-4}$	$6.7 \cdot 10^{-4}$
$\hat{E}_{rel}(\%)$	$7 \cdot 10^{-3}$	$1.6 \cdot 10^{-1}$	$8.8 \cdot 10^{-3}$	$3.4 \cdot 10^{-3}$
\hat{E}_{abs}	$3.1 \cdot 10^{-5}$	$6.3 \cdot 10^{-4}$	$2.4 \cdot 10^{-4}$	$8.1 \cdot 10^{-4}$
$E_{rel}^{max}(\%)$	1.16	1.6	0.9	0.5
E_{abs}^{max}	$4.6 \cdot 10^{-3}$	$5.4 \cdot 10^{-3}$	$2.5 \cdot 10^{-2}$	$7.5 \cdot 10^{-3}$
$Q_{1\%}(\%)$	99.7	99.7	100	99.7
$Q_{0.1\%}(\%)$	98.8	43.6	97.9	92.9

Table 3 Results for the approximation of λ_{cr} for non-orthotropic laminates for combined loading and pure shear loading

Loading Type	Combined loading		Pure shear loading	
	MOQ	ANN	MOQ	ANN
MSE	$6.9 \cdot 10^{-4}$	$2.7 \cdot 10^{-4}$	$1.7 \cdot 10^{-4}$	$9.3 \cdot 10^{-4}$
LOF(%)	$3 \cdot 10^{-2}$	$1.2 \cdot 10^{-2}$	$3.4 \cdot 10^{-4}$	$1.9 \cdot 10^{-3}$
$\hat{E}_{rel}(\%)$	$7.7 \cdot 10^{-2}$	$1.4 \cdot 10^{-1}$	$3 \cdot 10^{-2}$	$7.6 \cdot 10^{-2}$
\hat{E}_{abs}	$6.4 \cdot 10^{-3}$	$1.2 \cdot 10^{-2}$	$7 \cdot 10^{-3}$	$1.8 \cdot 10^{-2}$
$E_{rel}^{max}(\%)$	5.1	1.3	0.47	0.9
E_{abs}^{max}	$3.8 \cdot 10^{-1}$	$8.8 \cdot 10^{-2}$	$8.9 \cdot 10^{-2}$	0.15
$Q_{1\%}(\%)$	98.2	99.8	100	100
$Q_{0.1\%}(\%)$	89	48.1	93.1	79.9

5.2 Approximation models for varying loading conditions

Based on the observations previously made, λ_{cr} is approximated through its reciprocal, the result of the approximation is then inverted and the accuracy is measured on λ_{cr} . For the first case (no shear), $N = 468$ points were used with $N_x \in [-100, 0]$ and $N_y = [-50, 50]$ and for the second case 940 points were used with $N_x \in [-100, 0]$, $N_y = [-50, 50]$ and $N_{xy} = [0, 50]$. In both cases, the stacking sequence that was fixed was a non-orthotropic one $[-45/-45/0/45/90/-45/0]_S$ (2×7 plies). Results are in Tab. 4. In that case, mixture of quadratic models performs better for all accuracy metrics. Quantiles measures and quantile curves (see Fig. 8 a) and 8 b)) show the same tendency as in the former test cases. Mixture models are much more accurate for a large number of points of the validation basis.

5.3 Approximation models in the general case

In that case, we make both stacking sequence and loading vary. We distinguish two cases. In the first one, we consider non-orthotropic laminates and no shear loading (bi-axial loading including tension/compression). Dimension of regression in that case is 5: ξ_D^1 , ξ_D^2 , ξ_D^3 , N_x and N_y . We used 5400 points ranging in Miki's tetrahedron for lamination parameters and $N_x \in [-100, 0]$ and

Table 4 Results for the approximation of λ_{cr} for varying loadings (bi-axial loading and combined loading) and fixed SS

Loading Type	Bi-axial loading		Combined loading	
	MOQ	ANN	MOQ	ANN
MSE	$1.93 \cdot 10^{-6}$	$4.8 \cdot 10^{-5}$	$3.6 \cdot 10^{-3}$	$6.6 \cdot 10^{-3}$
LOF(%)	$2.1 \cdot 10^{-4}$	$5 \cdot 10^{-3}$	$2.6 \cdot 10^{-1}$	$4.7 \cdot 10^{-1}$
$\hat{E}_{rel}(\%)$	$5.1 \cdot 10^{-3}$	$9.3 \cdot 10^{-2}$	$4 \cdot 10^{-1}$	$7.1 \cdot 10^{-1}$
\hat{E}_{abs}	$1 \cdot 10^{-4}$	$2 \cdot 10^{-3}$	$1.1 \cdot 10^{-2}$	$1.7 \cdot 10^{-2}$
$E_{rel}^{max}(\%)$	1.4	2	11.1	29.4
E_{abs}^{max}	$3.9 \cdot 10^{-2}$	$9.9 \cdot 10^{-2}$	1.1	1.1
$Q_{1\%}(\%)$	99.9	99.4	90.4	81.8
$Q_{0.1\%}(\%)$	98.8	75.6	65.9	28.9

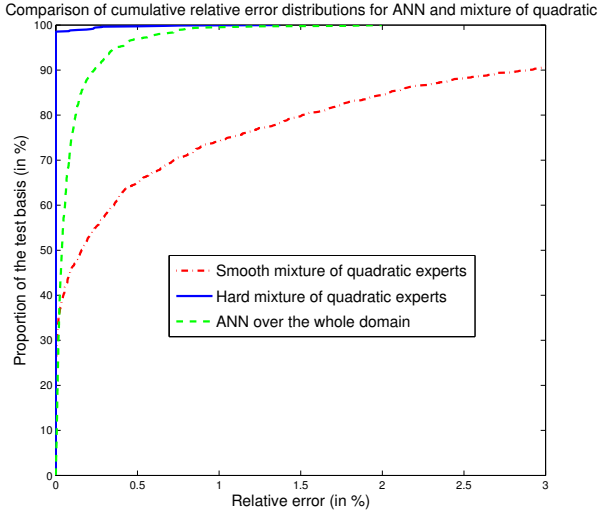
Table 5 Results for the approximation of λ_{cr} for varying non-orthotropic laminates and for varying flux

Loading Type	Bi-axial loading		Combined loading	
	MOR	ANN	MOR	ANN
MSE	$7.6 \cdot 10^{-3}$	$3.4 \cdot 10^{-3}$	$1.9 \cdot 10^{-2}$	$7 \cdot 10^{-3}$
LOF(%)	$3.8 \cdot 10^{-1}$	$1.7 \cdot 10^{-1}$	$3.8 \cdot 10^{-1}$	$1.3 \cdot 10^{-1}$
$\hat{E}_{rel}(\%)$	0.9	1.6	0.67	1.25
\hat{E}_{abs}	$3.2 \cdot 10^{-2}$	$3.6 \cdot 10^{-2}$	$3.3 \cdot 10^{-2}$	$3.7 \cdot 10^{-2}$
$E_{rel}^{max}(\%)$	20.9	40.5	31	22.4
E_{abs}^{max}	1.23	0.7	3.64	1.56
$Q_{1\%}(\%)$	73.7	43.6	84.6	55.6
$Q_{0.1\%}(\%)$	19.5	4.1	28.6	6.6

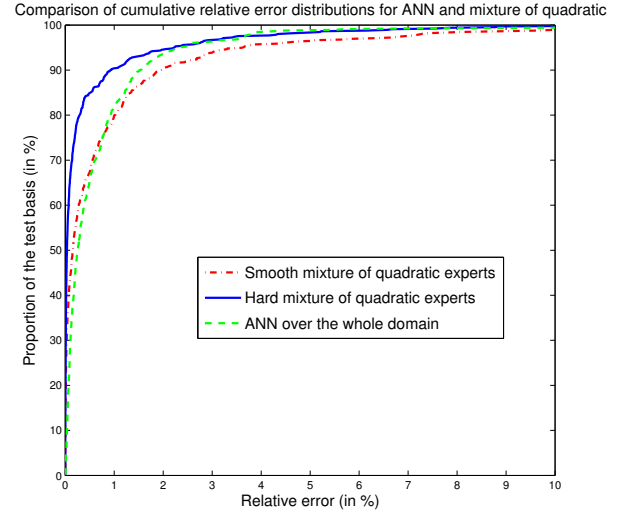
$N_y \in [-50, 50]$. In the second, we added shear loading, dimension of regression was then 6 and we used 8400 points within the same domain with $N_{xy} \in [0, 50]$. Results are in Tab. 5 and in Fig. 8 c) and 8 d). For both regressions, results show that ANN's give lower MSE, but for all the other accuracy metrics, the mixture of rational experts gives a better accuracy. Regarding quantile errors, we have the same tendency as in the other cases, that is mixture models gives a better accuracy for most points than ANN's.

5.4 Conclusion on the accuracy of the approximation

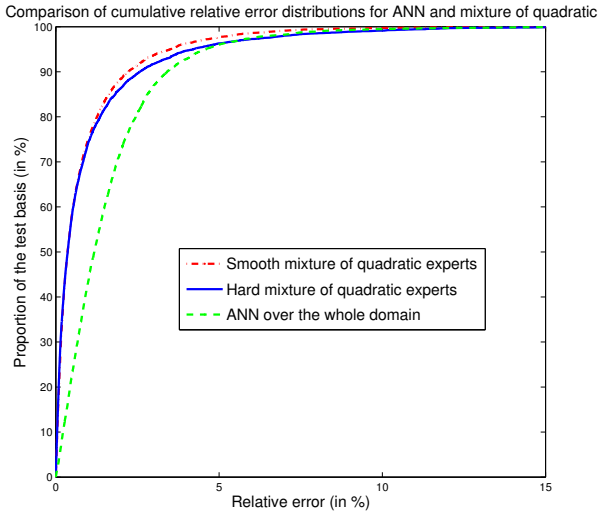
We see that in many cases, mixture models offers quite a good performance in terms of the accuracy of the approximation. For most cases, the hard recombination was found to be better than the smooth recombination and a reasonably good artificial neural network. In case one type of variables, amongst stacking or loading, is fixed, the accuracy is very high allowing to use the approximation models within an optimization process (see section 6). When material and loading vary the quality of the approximation is degraded, this is of course due to the dimension but also of the growing complexity of λ_{cr} ; much modes are indeed covered when making material and loading vary. What suggests these results is that approximation models should take advantage of this mode-based structure to improve the



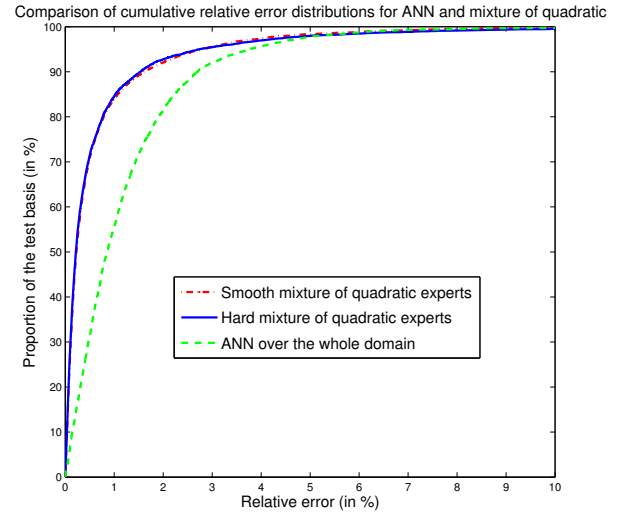
(a) Comparison of approximations of λ_{cr} over N_x and N_y for a non-orthotropic laminate



(b) Comparison of approximations of λ_{cr} over N_x , N_y and N_{xy} for a non-orthotropic laminate



(c) Comparison of approximations of λ_{cr} over ξ_D^1 , ξ_D^2 , ξ_D^3 , N_x and N_y



(d) Comparison of approximations of λ_{cr} over ξ_D^1 , ξ_D^2 , ξ_D^3 , N_x , N_y and N_{xy}

Fig. 8 Quantile curves for the approximation of λ_{cr} a) over N_x and N_y b) over N_x , N_y and N_{xy} c) over ξ_D^1 , ξ_D^2 , ξ_D^3 , N_x and N_y d) ξ_D^1 , ξ_D^2 , ξ_D^3 , N_x , N_y and N_{xy}

accuracy of the approximation. However, doing so requires a fairly good number of learning points within each mode, which is not an easy task to obtain without prior knowledge.

6 Applications to optimization

6.1 Optimization problem

In order to illustrate the interest of the approximation of λ_{cr} , we consider a stacking sequence optimization to

maximize critical buckling factor of a composite plate under combined loading. The optimization problem can be stated as follows

$$\begin{cases} \max \lambda_{cr}(\xi_D^1, \xi_D^2, \xi_D^3) \\ \text{s.t.} & 2|\xi_D^1| - \xi_D^2 - 1 \leq 0 \\ & 2|\xi_D^3| + \xi_D^2 - 1 \leq 0 \end{cases}$$

where some parameters are fixed: the material, the dimensions of the plate a and b , the total number of plies n , the loading with N_x , N_y and N_{xy} .

6.2 Description of the two distinct approaches

Two approaches will be compared to solve this problem:

- an explicit approach: it consists in listing all the feasible stacking sequences for a fixed number of plies n and computing the buckling load with a Rayleigh-Ritz method. The optimization problem is written as follows

$$\max_{\text{feasible SS}} \lambda_{cr}(\text{SS})$$

where the acceptable stacking sequence space is generated by listing the whole of the possible combinations of angles $[0^\circ, \pm 45^\circ, 90^\circ]$ which comply with the manufacturing rules (see section 2.2). The critical buckling factor λ_{cr} is computed with a Rayleigh-Ritz (RR) method on the subset of feasible stacking sequences. The optimal stacking sequence SS^* is referred to as the reference solution for the optimization problem.

- a two-step approach composed of a continuous optimization in the out-of-plane lamination parameters space followed by a post-identification to find the associated optimal stacking sequence.

1. Solve the continuous optimization problem

$$\begin{cases} \max \lambda_{cr}(\xi_D^1, \xi_D^2, \xi_D^3) \\ \text{s.t.} & 2|\xi_D^1| - \xi_D^2 - 1 \leq 0 \\ & 2|\xi_D^3| + \xi_D^2 - 1 \leq 0 \end{cases}$$

and determine the optimal out-of-plane lamination parameters $(\xi_D)^* = (\xi_D^1, \xi_D^2, \xi_D^3)^*$. The concavity of λ_{cr} ensures that any local maximum is a global maximum and that a gradient-based methods (such as SQP,...) will converge to a global maximum⁴.

2. From the optimal vector $(\xi_D)^*$ find the associated SS^* by solving

$$\begin{cases} \max \lambda_{cr}(\text{SS}) \\ \text{s.t.} & \xi_D(\text{SS}_{\text{feasible}}) \in \mathcal{N}((\xi_D)^*) \end{cases}$$

where $\mathcal{N}((\xi_D)^*)$ denotes the neighborhood of the optimal vector $(\xi_D)^*$. To define this neighborhood, we consider the ball $\mathcal{B}((\xi_D)^*, r)$ of center $(\xi_D)^*$ and of radius r chosen such that the

cardinal of points inside \mathcal{B} is equal to 20 (fixed number). The reason for choosing the best stacking within a neighborhood is again related to the concavity of λ_{cr} . Indeed, this ensures that the discrete optimum can not be too far away from the continuous optimum. There is no reason however that the discrete optimum corresponds to the closest discrete stacking sequence. This local research could definitely be improved by constructing a new distance that will weight the influence of each ξ_D^i (based on the Hessian of λ_{cr} at the optimum for instance).

6.3 Comparison of the optimization results

We consider the Graphite/Epoxy material given in Tab. 1, a plate of 650×250 mm with 10×2 plies according to the symmetry. A piecewise polynomial regression of degree 2 (MOQ) is built to approximate the critical buckling factor λ_{cr} and is used in the optimization process to reduce computational time (compared with the RR approach).

6.3.1 A combined loading example

First the combined loading $N_x = -50N.mm^{-1}$, $N_y = 20N.mm^{-1}$ and $N_{xy} = 20N.mm^{-1}$ is considered. We report in Tab. 6 the results obtained with the two approaches: in all cases we obtained the same optimal stacking sequence, the only difference results in the number of objective function evaluations: 7032 by listing all the feasible subset of stacking sequences with 10×2 plies, 269 function evaluations for the continuous optimization by using the two-step approach with the RR method to compute λ_{cr} instead of 39 evaluations with the MOQ approximation. For the SS-identification process, 20 more evaluations of λ_{cr} are required to build the neighborhood $\mathcal{B}((\xi_D)^*, r)$ of the optimal vector and then choose the optimal stacking sequence.

The convergence of the optimization process is compared on Fig. 9. Due to the smoothness of the quadratic approximate model (MOQ), the number of iterations is drastically reduced with 9 iterations instead of 21 with the RR method. Fig. 10 shows the feasible out-of-plane lamination parameters in Miki'tetrahedron. The considered neighborhood of the continuous solution is also represented and contains the feasible optimal solution. As expected, we can see that these optimal parameters are on the boundary of the domain. The use of a piecewise polynomial approximation of the λ_{cr} offers many advantages in term of convergence, computing time and makes it possible in this case to find the reference solution.

⁴ Convergence cannot be simply ensured because of the non-differentiability of the objective function. In reality, this problem is a typical non smooth optimization problem (being formally a maximization problem of an objective function computed through a minimization problem). Optimality conditions need a more general definition for the gradient (such as Clarke's subdifferential, see [27], [31]) and well-posedness and convergence can be shown for this particular problem where the objective function is a piecewise differentiable concave function. We did not use here such optimality conditions nor specific algorithms for non smooth optimizations (e.g Shor's algorithm)

	explicit	2-step with RR	2-step with MOQ
optimal SS	$[-45/-45/-45/0/45/45/0/0/45/90]_s$		
Error at optimum (%)	exact	exact	0.03%
Number of λ_{cr} evaluations	7032	269 + 20	39 + 20

Table 6 Optimization result with the combined loading $N_x = -50N.mm^{-1}$, $N_y = 20N.mm^{-1}$ and $N_{xy} = 20N.mm^{-1}$.

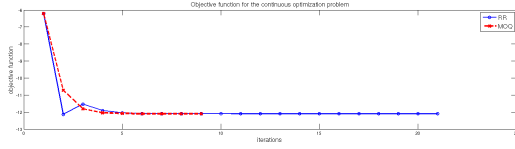


Fig. 9 Objective function during the optimization process with the combined load

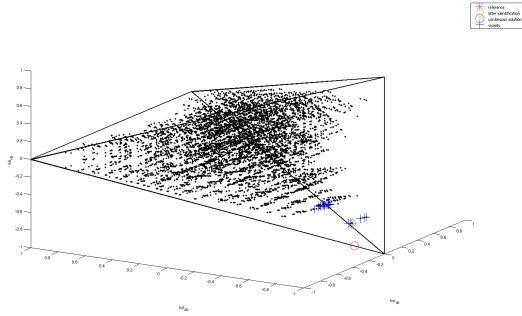


Fig. 10 Optimal solution in the lamination parameters space (the 7032 feasible ξ_D are illustrated by a black dot market) under the combined loading

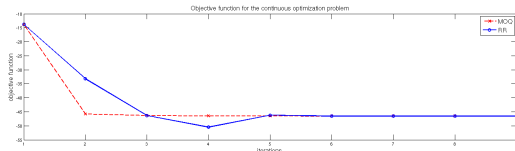


Fig. 11 Objective function during the optimization process with the shear loading

6.3.2 A pure shear loading example

To confirm these first very promising results, a second loading case is considered with $N_x = N_y = 0N.mm^{-1}$ and $N_{xy} = 20N.mm^{-1}$. The results are presented in Tab. 7. As previously, the reference stacking sequence is found by the two-step approach in both cases: with the RR method or the MOQ method to compute λ_{cr} . The number of iterations is very close and Fig. 11 confirms that the objective function converges in a similar way (8 or 9 iterations). One more time, the optimal solution belongs to the boundary of the Miki' tetrahedron as shown in Fig. 12.

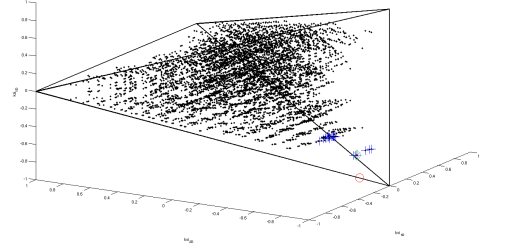


Fig. 12 Optimal solution in the lamination parameters space (the 7032 feasible ξ_D are illustrated by a black dot market) under the shear loading

6.4 Conclusion of the optimization applications

The use of our approximation model of λ_{cr} is particularly useful for the optimization strategy developed here. The approach in 2 stages with MOQ makes it possible to find the reference solution with few evaluations of the objective function, and in a negligible computational time. If the number of plies n would be higher, acceptable space would be larger and thus one could clarify all the combinations with difficulty. One will prefer in this case to use an evolutionary algorithm (genetic algorithm, ...) coupled with the MOQ approximation for the objective function to perform the stacking sequence identification.

7 Conclusions and perspectives

The behavior of the critical buckling load λ_{cr} for laminate composite plate was investigated. The dependence of λ_{cr} with respect to the stacking dependent lamination parameters was studied and shown to be concave. When considering internal load redistribution, the loading conditions vary it is therefore important to have a good approximation of λ_{cr} . It is shown that the reciprocal of λ_{cr} is easier to describe than λ_{cr} and then an approximation model of λ_{cr} building through the use of the reciprocal can achieve a reasonable accuracy. The basis of the approximation strategy used here takes advantage of the piecewise behavior of λ_{cr} and it is shown that piecewise approximation models based on simple model (linear, quadratic, rational) often performs bet-

	explicit	2-step with RR	2-step with MOQ
optimal SS	[-45/-45/-45/-45/90/45/45/45/45/0] _s		
Error at optimum (%)	exact	exact	0.1%
Number of λ_{cr} evaluations	7032	38 + 20	32 + 20

Table 7 Optimization result with the shear loading $N_x = N_y = 0N.mm^{-1}$ and $N_{xy} = 20N.mm^{-1}$.

ter than a sophisticated artificial neural network. More precisely, this piecewise approximation model seems to increase the approximation power for a large part of the validation bases, however a few points are misclassified leading to a large error for a small part of the validation bases. The accuracy of the approximation is often on the same range as an artificial neural network for global accuracy metrics (MSE) but for relative error distribution based metrics, piecewise models are much more accurate. When used within an optimization process, these piecewise models show very good performance, since it gives the same stacking sequence as the discrete optimization process and it seems to converge faster than the optimization based on the real buckling computations. As noticed in [7] one of the drawbacks of that piecewise modeling is that it may require quite a lot of points to correctly detect and grasp regions where λ_{cr} behaves simply.

One way of improvement for that technique would be to consider the gradient of the function to approximate directly in the clustering since the regions of λ_{cr} are totally disconnected which would make the clustering even easier. Another way would be to build directly the more appropriate local model, for instance, for low shear combined loadings, linear model gives very good accuracy but for high shear, the dependence seems more complicated and an adaptive strategy that automatically selects the local model (e.g amongst linear, sparse or full polynomial model) would definitely improve the method. Regarding potential applications, this technique is likely to be appropriate to build approximation model of optimization results. For instance, in a bilevel optimization framework, one often consider maximizing the critical buckling factor with respect to thickness and in-plane lamination parameters (or equivalently relative thicknesses). Such functions are known to be derivative-discontinuous and even discontinuous whenever discrete local optimization variables are addressed. This piecewise approximation model strategy would definitely be of great interest when building such approximation models. Another interesting area of application of such an approximation strategy would be structural optimization problems including aeroelasticity constraints and structural dynamics constraints where some of the quantities of interest are often computed

through an eigenvalue problem similar to the buckling equation. Regarding the specific area of the approximation of buckling computations, this technique would also be of great interest for any homogenized anisotropic materials and even inhomogeneous anisotropic material such as curved-fibers composites.

Acknowledgements The authors would like to thank Pr. A. Henrot and Pr. Z. Gürdal for their useful comments and discussions regarding buckling issues.

References

1. A.Y. Abu-Odeh and H.L. Jones. Optimum design of composite plates using response surface method. *Composite structures*, 43(3):233–242, 1998.
2. L.D. Akulenko and S.V. Nesterov. *High precision methods in eigenvalue problems and their applications*. CRC Press, 2005.
3. S.S. Antman. Theodore von Kármán. *A Panorama of Hungarian Mathematics in the Twentieth Century I*, pages 373–382, 2006.
4. S.S. Antman and M. Renardy. *Nonlinear problems of elasticity*. Springer, 2005.
5. M.S. Ashbaugh. Isoperimetric and universal inequalities for eigenvalues. In *Spectral theory and geometry: ICMS Instructional Conference, Edinburgh 1998*, page 95. Cambridge Univ Pr, 1999.
6. M. Autio. Optimization of coupled thermal-structural problems of laminated plates with lamination parameters. *Structural and Multidisciplinary Optimization*, 21(1):40–51, 2001.
7. D. Bettebghor, N. Bartoli, S. Grihon, J. Morlier, and M. Samuelides. Surrogate modeling approximation using a mixture of experts based on EM joint estimation. *Structural and Multidisciplinary Optimization*, pages 1–17, 2011.
8. F. Bloom and D. Coffin. *Handbook of thin plate buckling and postbuckling*. CRC Press, 2000.
9. MW Bloomfield, CG Diaconu, and PM Weaver. On feasible regions of lamination parameters for lay-up optimization of laminated composites. *Proceedings of the Royal Society A: Mathematical, Physical and Engineering Science*, 465(2104):1123, 2009.
10. R. Courant. Variational methods for the solution of problems of equilibrium and vibrations. *LECTURE NOTES IN PURE AND APPLIED MATHEMATICS*, pages 1–1, 1994.
11. M. Dauge and M. Suri. On the asymptotic behaviour of the discrete spectrum in buckling problems for thin plates. *Mathematical methods in the applied sciences*, 29(7):789–817, 2006.
12. F. De Gournay. *Optimisation de formes par la méthode des courbes de niveaux*. 2005.

13. C.G. Diaconu, M. Sato, and H. Sekine. Feasible region in general design space of lamination parameters for laminated composites. *AIAA journal*, 40(3):559–565, 2002.
14. J. Friedman, T. Hastie, and R. Tibshirani. The elements of statistical learning, 2001.
15. H. Fukunaga, H. Sekine, M. Sato, and A. Iino. Buckling design of symmetrically laminated plates using lamination parameters. *Computers & structures*, 57(4):643–649, 1995.
16. J.L. Grenestedt. A study on the effect of bending-twisting coupling on buckling strength. *Composite structures*, 12(4):271–290, 1989.
17. J.L. Grenestedt. Composite plate optimization only requires one parameter. *Structural and Multidisciplinary Optimization*, 2(1):29–37, 1990.
18. J.L. Grenestedt. Layup optimization against buckling of shear panels. *Structural and Multidisciplinary Optimization*, 3(2):115–120, 1991.
19. R.T. Haftka and Z. Gürdal. *Elements of structural optimization*. Kluwer Academic Pub, 1992.
20. P.N. Harrison, R. Le Riche, and R.T. Haftka. Design of stiffened composite panels by genetic algorithm and response surface approximations. In *AIAA/ASME/ASCE/AHS/ASC Structures, Structural Dynamics and Materials Conference, 36 th and AIAA/ASME Adaptive Structures Forum, New Orleans, LA*, pages 58–68, 1995.
21. A. Henrot. *Extremum problems for eigenvalues of elliptic operators: Antoine Henrot*. Birkhauser, 2006.
22. J.E. Herencia, R.T. Haftka, P.M. Weaver, and M.I. Friswell. Lay-up optimization of composite stiffened panels using linear approximations in lamination space. *AIAA Journal*, 46(9):2387–2391, 2008.
23. J.E. Herencia, P.M. Weaver, and M.I. Friswell. Optimization of anisotropic composite panels with T-shaped stiffeners including transverse shear effects and out-of-plane loading. *Structural and Multidisciplinary Optimization*, 37(2):165–184, 2008.
24. F.X. Irisarri. Stratégies de calcul pour l’optimisation multiobjectif des structures composites. 2009.
25. F.X. Irisarri, D.H. Bassir, N. Carrere, and J.F. Maire. Multiobjective stacking sequence optimization for laminated composite structures. *Composites Science and Technology*, 69(7-8):983–990, 2009.
26. F.X. Irisarri, F. Laurin, F.H. Leroy, and J.F. Maire. Computational strategy for multiobjective optimization of composite stiffened panels. *Composite structures*, 93(3):1158–1167, 2011.
27. K.C. Kiwiel. *Methods of descent for nondifferentiable optimization*. Springer-Verlag Berlin, 1985.
28. W.T. Koiter. Elastic stability and post-buckling behavior. *Nonlinear Problems*, pages 257–275, 1962.
29. L.P. Lebedev and I.I. Vorovich. *Functional analysis in mechanics*. Springer Verlag, 2003.
30. S.G. Lekhnitskii. Anisotropic plates. Technical report, DTIC Document, 1968.
31. A. Lewis. Eigenvalues and nonsmooth optimization. *LONDON MATHEMATICAL SOCIETY LECTURE NOTE SERIES*, 331:208, 2006.
32. M. Miki. A graphical method for designing fibrous laminated composites with required in-plane stiffness. *Japan Society for Composite Materials, Transactions*, 9:51–55, 1983.
33. M. Miki and Y. Sugiyama. Optimum design of laminated composite plates using lamination parameters. In *AIAA/ASME/ASCE/AHS/ASC Structures, Structural Dynamics, and Materials Conference, 32 nd, Baltimore, MD, Technical Papers. Pt. 1*, volume 8, 1991.
34. J.N. Reddy. *Mechanics of laminated composite plates and shells*, volume 2. CRC press, 2004.
35. B. Rousselet and D. Chenais. Continuité et différentiabilité d’éléments propres: application à l’optimisation de structures. *Applied Mathematics and Optimization*, 22(1):27–59, 1990.
36. C.P. Simon and L. Blume. *Mathematics for economists*, volume 7. Norton, 1994.
37. G. Soremekun, Z. Gürdal, C. Kassapoglou, and D. Toni. Stacking sequence blending of multiple composite laminates using genetic algorithms. *Composite structures*, 56(1):53–62, 2002.
38. I. Stakgold. Branching of solutions of nonlinear equations. *SIAM review*, 13(3):289–332, 1971.
39. B. Szabó and G. Királyfalvi. Linear models of buckling and stress-stiffening. *Computer methods in applied mechanics and engineering*, 171(1):43–59, 1999.
40. Y. Terada, A. Todoroki, and Y. Shimamura. Stacking sequence optimizations using fractal branch and bound method for laminated composites. *JSME International Journal Series A*, 44(4):490–498, 2001.
41. A. Todoroki and M. Sasai. Stacking sequence optimizations using GA with zoomed response surface on lamination parameters. *Advanced Composite Materials*, 11(3):299–318, 2002.
42. A. Todoroki, K. Suenaga, and Y. Shimamura. Stacking sequence optimizations using modified global response surface in lamination parameters. *Advanced Composite Materials*, 12(1):35–55, 2003.
43. G.J. Turvey. *Buckling and postbuckling of composite plates*. Springer, 1995.
44. M. Walker, S. Adali, and V. Verijenko. Optimization of symmetric laminates for maximum buckling load including the effects of bending-twisting coupling. *Computers & structures*, 58(2):313–319, 1996.
45. J.M. Whitney. The effect of transverse shear deformation on the bending of laminated plates. *Journal of Composite Materials*, 3(3):534, 1969.

A Quasiconcave functions and homogeneous functions

We recall here some basic definitions and properties of quasiconcave functions and homogeneous functions. In particular, we also give the Euler identity formula for homogeneous functions. Let $f : V \mapsto \mathbb{R}$ defined over a convex subset V of a vector space, f is *quasiconcave* if

$$\forall x, y \in V \quad \forall \theta \in (0, 1) f(\theta x + (1 - \theta)y) \geq \min(f(x), f(y)) \quad (45)$$

or equivalently, a quasiconcave function can be defined in terms of *upper level sets* $S_\alpha = \{x \in V | f(x) \geq \alpha\}$ that is, f is quasiconcave if for any $\alpha \in \mathbb{R}$, S_α is a convex set. This is the definition we used in this article. Quasiconcavity (and quasiconvexity) are a generalization of the well known concavity, a concave function is quasiconcave. Quasiconcave functions often appear in economics (e.g Cobb-Douglas function), game theory and optimization. These are assumptions for the min-max theorem.

Let $f : U \mapsto V$ a function defined a vector space U that maps to another vector space V . f is said to be *positive homogeneous* of degree α whenever

$$\forall x \in U \quad \forall \kappa \in \mathbb{R}^+ \quad f(\kappa x) = \kappa^\alpha f(x) \quad (46)$$

Linear functions are homogeneous functions of degree 1, the determinant function over $n \times n$ matrices is homogeneous of degree n . One important feature of homogeneous functions whenever they are continuously differentiable is that they admit the Euler identity characterization. $f : \mathbb{R}^n \mapsto \mathbb{R}$ is a positive homogeneous functions if and only if

$$\forall x \in \mathbb{R}^n \quad \sum_{i=1}^n x_i \frac{\partial f}{\partial x_i} = \alpha f(x) \quad (47)$$

To obtain (47), we simply differentiate (46) at κx with respect to κ to get

$$\sum_{i=1}^n x_i \frac{\partial f(\kappa x)}{\partial x_i} = \alpha \kappa^{\alpha-1} f(x). \quad (48)$$

It is worth noting that, if F is homogeneous of degree α and continuously differentiable, then its derivative is homogeneous of degree $\alpha - 1$. We end up with the following useful property, whose proof together with a lot of results and examples on quasiconcave and homogeneous functions can be found in [36]. Let f be a homogeneous function of degree 1 and quasiconcave then f is concave.

B Rayleigh-Ritz approximation for buckling and sensitivity analysis

We briefly recall here the Rayleigh-Ritz method for buckling computations. Note that, Rayleigh-Ritz methods are also widely used in structural dynamics, vibrations, quantum chemistry,... The main idea is to write the solution of a partial differential equation system or eigenproblem as a linear combination of test functions. Unlike finite element methods, the test functions are defined over the whole domain and satisfy boundary conditions. These basis functions are usually based on a closed-form solutions of a close unperturbed problem. This means that Rayleigh-Ritz methods are used when solving a pde or eigenproblem close in some sense (simple geometry, simple differential operator) to a simple one and are not as general as finite element methods. They are also close to spectral methods in the sense the test functions are defined over the whole domain and their convergence properties are usually quite good whenever the problem remains close to an original simple problem. In addition to that, as in spectral methods, the discretization step leads to dense matrices and high accuracy can be achieved with much less degrees-of-freedom than in finite elements methods.

Consider the following eigenproblem under its variational form: find $\lambda \in \mathbb{R}$ and $u \in \mathcal{V} - \{0\}$ (a Hilbert space) such that

$$a(u, u) - \lambda b(u, u) = 0 \quad (49)$$

with prescribed boundary conditions (e.g $u = 0$ on the boundary of the domain), with a and b being bilinear symmetric forms defined over \mathcal{V} , for sake of simplicity we will assume that they are both coercive and restrict ourselves to eigenproblems. The minmax theorem (or variational characterization) for eigenvalues are local minima of the Rayleigh ratio

$$R(u) = \frac{a(u, u)}{b(u, u)} \quad (50)$$

To ensure unicity of eigenmodes, it is convenient to add a normalization condition⁵ over u (see [19], e.g $b(u, u) = 1$, $\|b\|_\infty = 1$). Let's take $b(u, u) = 1$. The process of computing eigenvalues and eigenmodes of Eq. (49) boils down to solving the following problem

$$\begin{aligned} \min_{u \in \mathcal{V}} \quad & R(u) \\ \text{s.t} \quad & b(u, u) = 1 \end{aligned} \quad (51)$$

Instead of solving problem (51), we solve it over a finite-dimensional space \mathcal{V}_N . Consider (u_1, \dots, u_N) the basis of $\mathcal{V}_N \subset \mathcal{V}$ and let's denote for $v \in \mathcal{V}_N$

$$v(x, c) = \sum_{i=1}^N c_i u_i(x) \quad (52)$$

$$a(v, v) = a_N(c) = \sum_{i,j=1}^N a_{ij} c_i c_j \quad (53)$$

with

$$a_{ij} = a(u_i, u_j) \quad (54)$$

and

$$b(v, v) = b_N(c) = \sum_{i,j=1}^N b_{ij} c_i c_j \quad (55)$$

with

$$b_{ij} = b(u_i, u_j) \quad (56)$$

and denote by A and B the (symmetric positive definite) matrices of elements $(a_{ij})_{1 \leq i,j \leq N}$ and $(b_{ij})_{1 \leq i,j \leq N}$. We can write the KKT optimality conditions of problem (51) over \mathbb{R}^N

$$\min_{c \in \mathbb{R}^N | b_N(c)=1} a_N(c) \quad (57)$$

and so $c \in \mathbb{R}^N$ a local minimum of problem (57) necessary satisfies the following conditions (any point satisfying these conditions is also a local minimum since a_N and b_N are convex)

$$\frac{1}{2} \nabla a_N(c) - \lambda \nabla b_N(c) = (A - \lambda B)c = 0 \quad (58)$$

with

$$b_N(c) = c^t B c = 1 \quad (59)$$

And the linear equation defined by Eq. (58) has a nontrivial solution if and only if

$$\det(A - \lambda B) = 0 \quad (60)$$

that the Lagrange multiplier λ is an eigenvalue of A relatively to B .

To make this method more clear, let's take the example of composite plate buckling. As outlined in this paper, for simple geometry like plate, there exists a closed-form solution

⁵ This is indeed necessary to ensure unicity of the eigenmodes, since they are defined up to a multiplicative constant. This is even more critical when we have to compute the derivatives of the eigenmodes.

whenever the laminate is orthotropic and the loading is biaxial. In that case, buckling equation boils down to

$$D_{11} \frac{\partial^4 w}{\partial x^4} + D_{22} \frac{\partial^4 w}{\partial y^4} + 2(D_{12} + 2D_{66}) \frac{\partial^4 w}{\partial x^2 \partial y^2} = N_x \frac{\partial^2 w}{\partial x^2} + N_y \frac{\partial^2 w}{\partial y^2} \quad (61)$$

Closed form solution of Eq. (61) are obtained considering the following test functions

$$w_{ij}(x, y) = \sin(i\pi/x) \sin(j\pi/y) \quad (62)$$

and writing Eq. (61) we obtain the corresponding eigenvalues λ_{ij} as defined in Eq.(12). We therefore use $(w_{ij})_{i,j \in [1, N]}$ as test functions, leading to matrices A and B of size $N^2 \times N^2$ defined as

$$A_{(i-1)N+j, (k-1)N+l} = a_D(w_{ij}, w_{kl}) \quad (63)$$

and

$$B_{(i-1)N+j, (k-1)N+l} = b_N(w_{ij}, w_{kl}) \quad (64)$$

and λ_{cr} is found as the smallest positive eigenvalue of A relatively to B . It is worth noting here that when making the parameters of that buckling computation vary, there is no need to reassemble each time the full matrices A and B . One easy way to save computation is to assemble elementary matrices once for all such that for instance

$$A_D = D_{11}A_{11} + \dots + D_{16}A_{16} \quad (65)$$

where A_{ij} are matrices of size $N^2 \times N^2$ computed while performing the first analysis. This allows to perform new computations for new values of D faster, since the assembly becomes negligible and the main part of the computations lies in the eigensolver.

Suppose now we want to compute the sensitivity of λ_{cr} w.r.t to any design variable x , we have

$$\frac{\partial \lambda_{cr}}{\partial x} = w_{cr}^T \left(\frac{\partial A}{\partial x} + \lambda_{cr} \frac{\partial B}{\partial x} \right) w_{cr} \quad (66)$$

with w_{cr} the associated eigenvector whenever λ_{cr} is simple.

C Buckling space for loading conditions

In Fig. 6 we see that some values of (N_x, N_y, N_{xy}) do not give rise to buckling. In both plots we observe a 'hole' for which buckling analysis gives either a negative critical buckling factor or an infinite value. This is related to the assumption that the bilinear form $b_N(\cdot, \cdot)$ has at least one positive direction, i.e a displacement w such that $b_N(w, w) > 0$. This assumption ensures that there exists at least one eigenvalue $\lambda > 0$, the positive part of the spectrum is not empty. In the literature concerned with linear buckling in the frame of three-dimensional linear elasticity ([11], [39]), this condition is written over the stress tensor and is referred to as *non-negativity property*. The aim of that section is to show that this assumption naturally explains the 'non-buckling' area in the loading conditions space.

The bilinear form $b_N(\cdot, \cdot)$ is

$$b_N(u, u) = - \iint_{\Omega} N_x \frac{\partial u^2}{\partial x} + N_y \frac{\partial u^2}{\partial y} + N_{xy} \frac{\partial u}{\partial x} \frac{\partial u}{\partial y} dx dy \quad (67)$$

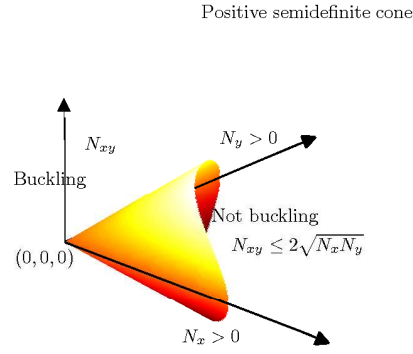


Fig. 13 Buckling and non-buckling zones in loading space

Eq. (67) can be written in a matrix form

$$b_N(u, u) = - \iint_{\Omega} \left(\frac{\partial u}{\partial x} \frac{\partial u}{\partial y} \right) \begin{pmatrix} N_x & \frac{N_{xy}}{2} \\ \frac{N_{xy}}{2} & N_y \end{pmatrix} \begin{pmatrix} \frac{\partial u}{\partial x} \\ \frac{\partial u}{\partial y} \end{pmatrix}^T dx dy \quad (68)$$

and the non-negativity property is satisfied whenever the forces tensor N

$$N = \begin{pmatrix} N_x & \frac{N_{xy}}{2} \\ \frac{N_{xy}}{2} & N_y \end{pmatrix} \quad (69)$$

has at least one negative eigenvalue. This ensures that there exists a positive eigenvalue and that $\lambda_1 \geq 0$. Equivalently, loading conditions do not give rise to buckling whenever tensor N is semidefinite positive. The buckling zone in (N_x, N_y, N_{xy}) is then the complement in \mathbb{R}^3 of the positive semidefinite cone. This then leads to the following conditions

- 1st case: either $N_x < 0$ or $N_y < 0$. In that case buckling occurs with no condition on N_{xy}
- 2nd case: in case $N_x \geq 0$ and $N_y \geq 0$, buckling occurs if

$$|N_{xy}| > 2\sqrt{N_x N_y}. \quad (70)$$

We depicted the buckling and non buckling zones and the positive semidefinite cone in Fig. 13 and 14. Now we can comment and explain the main part of the 'hole' in Fig. 6 when compared to the buckling/non-buckling zones in (θ, ϕ) space depicted Fig. 14. The rest of the hole can be explained by the fact as a discrete numerical approximation scheme was used, we could not explore all the different modes. Typically in our case, since 20×20 basis functions were used, modes with more than 21 half-waves along one direction can not be detected.

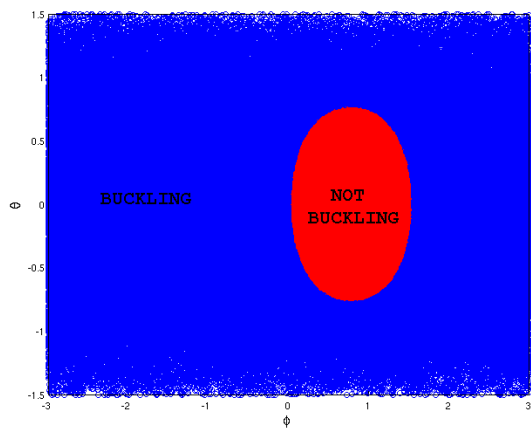


Fig. 14 Buckling and non-buckling zones in (θ, ϕ) space